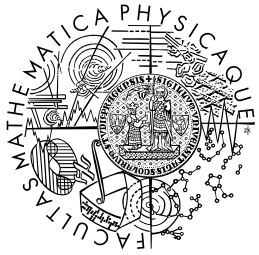

FACULTY
OF MATHEMATICS
AND PHYSICS
Charles University

MASTER THESIS

Bc. Lukáš Fusek

Study of CO and N_2 Interaction with Anode Catalysts of Proton-Exchange Membrane Fuel Cells

Department of Plasma and Surface Sciences

Supervisor of the master thesis: prof. RNDr. Vladimír Matolín, DrSc.

Study programme: Physics

Study branch: Physics of surfaces and ionized enviroments

Prague, 2019

I declare that I carried out this master thesis independently, and only with the cited sources, literature and other professional sources.

I understand that my work relates to the rights and obligations under the Act No. 121/2000 Sb., the Copyright Act, as amended, in particular the fact that the Charles University has the right to conclude a license agreement on the use of this work as a school work pursuant to Section 60 subsection 1 of the Copyright Act.

In Prague date May 10, 2019 Lukáš Fusek

I would like to thank my family and friends for all kind of support they have given me during my studies, my supervisor, prof. RNDr. Vladimir Matolin, DrSc., and consultant Mgr. Roman Fiala, PhD. for their patience, guidance and advice, and all colleagues at our department for a pleasant and friendly environment and willingness to help.

Title: Study of CO and N_2 Interaction with Anode Catalysts of Proton-Exchange Membrane Fuel Cells

Author: Bc. Lukáš Fusek

Department: Department of Plasma and Surface Sciences

Supervisor: prof. RNDr. Vladimír Matolín, DrSc., Departement of Plasma and Surface Sciences

Abstract: Poisoning of the catalyst seems to be one of the most serious problems preventing a widespread commercialization of fuel cell technology. This thesis focuses on the effect of CO poisoning and hydrogen dilution by nitrogen on performance of fuel cells with low platinum content. Catalysts were deposited by magnetron sputtering directly on membrane etched by plasma. Alloys with different platinum-ruthenium ratio were used to mitigate the CO poisoning. We found that presence of nitrogen has almost negligible effect on the fuel cell performance. On the other hand, CO, even in small concentrations, caused a significant drop in power density. PtRu with atomic ratio 2:1 and 1:1 showed the best CO tolerance.

Keywords: Proton-exchange membrane fuel cell, CO poisoning, Anode

Contents

1. Introduction

Fuel cell technology represents a very promising energy source for both static and mobile devices. It is based on the direct conversion of chemical energy of reactants into electricity, which results in high efficiency and low emissions. In particular in the case of hydrogen fuel cells, the only waste products are water and heat. However, the presence of a catalyst is required for the reaction to proceed. The most commonly used catalysts are platinum and alloys of platinum and another metal.

Despite the enormous scientific effort of the last decades, there are still unsolved problems hampering a widespread commercialization of fuel cells. One of them is poisoning of a catalyst by carbon species, especially carbon monooxide, which are present in the hydrogen as a residue of its fabrication. Nowadays, 96 % of the worldwide hydrogen production is based on fossil fuels [1], and thus the product is rich in carbon species.

The phenomenon of catalyst poisoning has been intensively studied since 90s [2]. The main problem lies in preferential adsorption of CO on catalytically active sites, creating a strong bond and blocking the reaction. A decrease in the reaction rate is drastically reduces the performance of the whole cell. Even a concentration in the order of few ppm of CO could have a dramatic effect on the fuel cell operation. There are a few methods of mitigation of CO poisoning. Addition of ruthenium, which enhance oxidation of adsorbed CO, is one of them.

In applications, air is supposed to play the role of an oxidizer. Nitrogen which is crossing through the membrane to the anode is supposed to be innert and cause only dilution of fuel. However, the effect of its presence on fuel cell performance has to be known.

The aim of this thesis is to study the effect of CO and nitrogen on fuel cell performance. Specifically, we focus on anodic processes and hydrogen oxidation reaction.

The goals of this thesis are:

1. To add a pannel for mixing gases with sufficient accuracy to our testing station;

2. To study the effect of CO and nitrogen on reference sample using commercial catalysts;

3. To prepare anodes with low platinum content by magnetron sputtering,

4. To test new anodes using commercial cathode;

5. To study the effect of ruthenium on CO tolerance of catalyst;

6. To analyze the results and compare them with the commercial reference and literature.

2. Fuel cells

2.1 History of fuel cells

Fuel cell technology represents a very propective, highly efficient and ecological source of energy. There has been a great effort to develop and commercialize this technology for last thirty years. However, the concept of a gaseous fuel cell is much older, it has been known for more than 150 years.

It was introduced for the first time, at the end of 1830s by a British jurist and amateur scientist sir William Grove. He found that it is possible to reverse the electrolysis of water by using an appropriate catalyst, and that electricity is produced during this process. Fig. 2.1 shows his schematic drawing published in 1839. He used a liquid electolyte instead of the polymer membrane commonly used nowadays, and platinum was used as a catalyst.

Three years later, he built the first fuel cell battery containing 50 platinum sheets in series. Performance of the battery was almost negligible, but Grove also stated that the main difficulty is to obtain "a notable surface of action" [4].

This simple idea of increasing the performence by increasing the active surface was followed at the end of the century by a German chemist Ludwig Mond and and British chemist Carl Langer. They proposed using a three-dimmensional porous structure of electrodes instead of two-dimmensional platinum foil. Unfortunately, it was the only significant progress made for almost a whole century. Except for Mond and Langer or Francis Thomas Bacon in the 20s and 30s, there was little interest in the fuel cell technology.

Everything changed at the end of 50s when a new direction of fuel cell development appeared. The liquid acid electrolyde was replaced by a solid acid electrolyte, which made it more compact and suitable for application. Even NASA noticed the potential of fuel cells and integrate them into the Gemini Project as a possible power source for space missions [5].

A great advantage of fuel cells was that water was the only waste product. Water could be in turn used by astronauts, which would lead to a decrease in mass of the load. Due to the collaboration of NASA and General Electric, a 1 kW

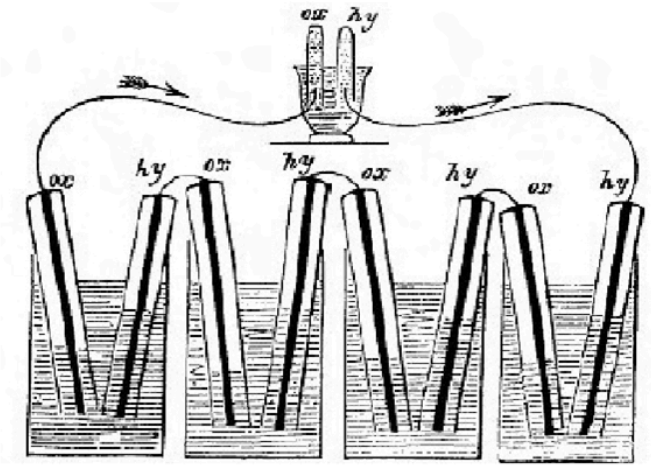

Figure 2.1: Original Grove's drawing published in 1839 *(Reprinted from [3])*

stack with a total weight of 29 kg was constructed. Even though the fuel cell stacks passed all tests successfully (e.g. Gemini II and Gemini V), the technology was replaced by silver-zinc batteries. However, NASA is nowadays considering a return to the fuel cells (e.g. Mars Flyer and another space vehicle projects) [6].

In the 60s, an important step in membrane development was made. In 1969 DuPont company announced that their research group lead by Frank Gresham discovered Nafion. It was "the first commercially produced perfluorinated ion exchange resin" [7] and for almost sixty years it is the most widespread membrane in fuel cell techologies.

All research mentioned above was done only for academic or special purposes such as space missions, especially due to the high cost of platinum. The real revolution happened in 1983 when Ballard Power System Inc. began working on fuel cell development for commercial use. Only in three years Ballard constructed a fuel cell stack operating on pressurized air and in 1993 they presented the first bus powered by fuel cell [8]. This was a beggining of a boom in this field and since then fuel cell technology has been subject to much interest and research. More than 9000 articles have been published in the last thirty years and the number is still growing.

2.2 Basic principle of a fuel cell

The fuel cell is based on the conversion of chemical energy of reactants to electrical energy. The overall reaction (2.1) of fuel cell could be described as a synthesis of hydrogen and oxygen yielding water as a product.

$$\mathrm{H_2} + \frac{1}{2}\mathrm{O_2} \rightarrow \mathrm{H_2O} \tag{2.1}$$

The reaction is exothermic as one can see from the enthalpy balance. The standard enthalpy of formation for hydrogen and oxygen molecule is zero by definition, for water it is $\Delta H^0 = -285.83\,\mathrm{kJ/mol}$ at liquid phase and $\Delta H^0 = -241.8\,\mathrm{kJ/mol}$ [9] at gaseous phase. Assuming constant pressure in the cell, the enthalpy change can be recalculated for arbitrary temperature using Kirchhoff's law,

$$\Delta H_T = \Delta H^0 + \int_{T_0}^{T} c_p(T)\mathrm{d}T, \tag{2.2}$$

where c_p is specific heat at constant pressure. Note, though, that the temperature dependence of c_p is usually supposed to be negligible within the small temperature range.

The fuel cell functions as follows, see Fig. 2.2. The fuel - hydrogen - is input to an anode, where it is oxydized. Anodic half reaction is

$$\mathrm{H_2} \rightarrow 2\mathrm{H^+} + 2\mathrm{e^-}. \tag{2.3}$$

Protons - hydrogen cations - pass through an ionic membrane to a cathode. Electrons, for which the membrane is non-conductive, are forced by potential difference to go to the collector plate and then through outer circuit to the cathode. At the cathode an oxygen is reduced:

$$\mathrm{O_2} + 4\mathrm{H^+} + 4\mathrm{e^-} \rightarrow 2\mathrm{H_2O}. \tag{2.4}$$

The produced water is taken away from the cell. The problematics of water management is crucial for high performance of the fuel cell [10, 11, 12, 13]. Membrane conductivity strongly depends on its hydration, therefore some water must be present in the cell. On the other hand, excess of water causes so-called flooding of an electrode. Water condensates in the pores and impedes the transport

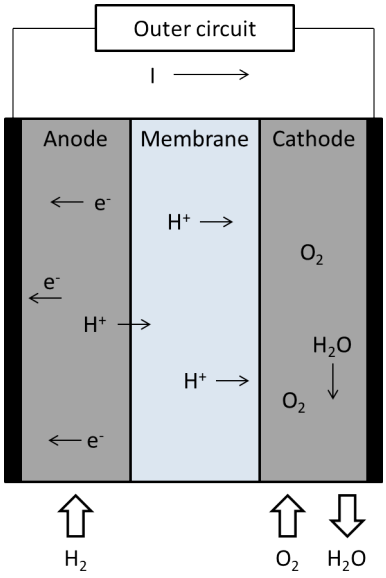

Figure 2.2: Schematic drawing of the fuel cell process

of oxygen to active sites. In addition, water covers the active sites, which leads to further decrease of electrochemical activity.

During the reaction (2.1) two electrons per reacting molecule of hydrogen are transfered from the anode to the cathode. The maximum current produced by the cell with constant fuel flow is given by

$$I_{\max} = \frac{1}{30000} \cdot \frac{QN_A e}{V_m}, \tag{2.5}$$

where Q is the flow of the fuel in standard cubic centimeters per minute, N_A is Avogadro's number, V_m is molar volume of a gas and e is elementary charge. Using fundamental constants, Eq. (2.5) can be written as

$$I_{\max} \approx 0.143Q. \tag{2.6}$$

According to this calculation, it is possible to say that 7 sccm of hydrogen is required for the current of 1 A. The situation described above assumes ideal condition when all hydrogen contributes to the current. In reality, however, some of the hydrogen passes through the cell unreacted and not even all reacted hydrogen contributes to the current. However, these losses are usually negligible. We thus define a fuel utitlization coefficient μ

$$\mu = \frac{\text{number of hydrogen molecules contributing to the current}}{\text{number of hydrogen molecules input to the cell}}. \tag{2.7}$$

Then the current generated by the cell is

$$I \approx 0.143 \mu Q. \tag{2.8}$$

The ideal cell voltage can be determined from termodynamics. Maximal useful energy, in this case electrical energy, is equal to the change of Gibbs free energy

$$\Delta G^0 = -nFE^0, \tag{2.9}$$

where n is number of moles of electrons involved in the reaction, F Faraday's constant, and E^0 reversible potential or ideal voltage of the fuel cell at standard condition. For reaction (2.1) is $\Delta G^0 = -237\,\mathrm{kJ/mol}$ for liquid water and $\Delta G^0 = -228\,\mathrm{kJ/mol}$ for vapor. The corresponding reversible potentials are $E^0 = 1.23\,\mathrm{V}$ and $E^0 = 1.18\,\mathrm{V}$, respectively [3, 14].

Temperature- and pressure-dependence of a reversible potential is given by Nernst's equation

$$E = E^0 + \frac{RT}{2F} \ln \frac{p_{\mathrm{H_2}} p_{\mathrm{O_2}}^{\frac{1}{2}}}{p_{\mathrm{H_2O}}}, \tag{2.10}$$

where p_a stands for partial pressure of gas a and R is the universal gas constant.

Real voltage of the cell is lower than the one calculated in Eq. (2.10). There are three main types of potential losses. The first one is caused by the activation of the reaction, its kinetics and the crossover effect. The second one corresponds to standard ohmic losses due to the resistance of the cell. The last one appears especially at high current densities and it is connected with the difussion properties of the electrodes and fuel transport.

Theoretical efficiency is defined as a ratio of maximal useful energy, i.e. change of Gibbs free energy, and total energy released during the reaction, i.e. change of enthalpy,

$$\eta = \frac{\Delta G}{\Delta H}. \tag{2.11}$$

Using values for the standard conditions we obtain $\eta^0 = 0.83$.

2.3 Structure of a fuel cell

As mentioned already in the previous part, a fuel cell consists of two electrodes and a membrane. This set up is usually called a membrane-electrode assembly

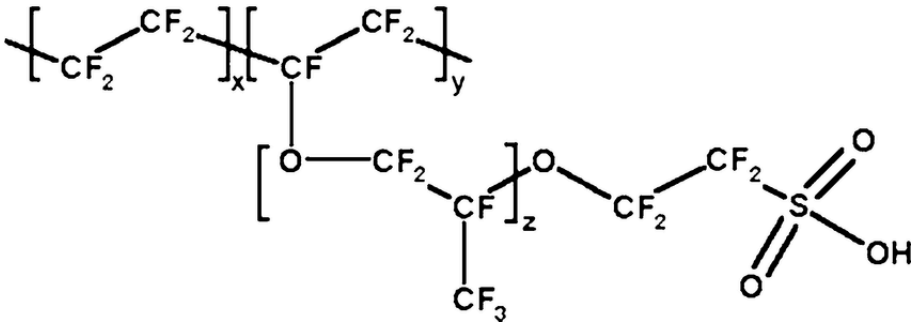

Figure 2.3: Chemical structure of Nafion *(Reprinted from [15])*

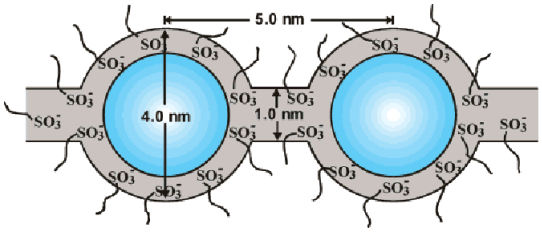

Figure 2.4: Schematic drawing of sulfonic acid network of Nafion *(Reprinted from [17])*

(MEA) and it is the most important part having a crucial impact on overall properties and performace of the fuel cell. As shown in Fig. 2.2, the two electrodes are attached to the membrane, one from each side. The membrane serves also as a separator of gases.

2.3.1 Membrane

The most often used membrane in both research and application is Nafion from DuPont company. It could be described as a copolymer where the main chain is similar to polytetrafluorethylene (PTFE) and perfluorated side chain is ended by sulfonic acid group, see Fig. 2.3. More specificaly it is copolymer of 1,1,2,2-tetrafluoroethene and 1,1,2,2-tetrafluoro-2-[1,1,1,2,3,3-hexafluoro-3-(1,2,2-trifluoroethenoxy)propan- 2-yl]oxyethanesulfonic acid [16].

Ion conductivity of the membrane is linked with sulfonic acid group SO_3H at the end of side chains. In the presence of water, it is converted to $SO_3^- - H_3O^+$ and according to small-angle X-ray scattering, it creates small spherical clusters with average size of 40 Å. These clusters are connected by short channels and create cluster network as shown in Fig. 2.4. The proton conductive cluster

network is surrounded by non-conductive fluorocarbons. Hydration of membrane has to be sufficient to reach percolation and therefore good proton conductivity of the membrane [17, 18].

Proton conductivity decreases with increasing thickness of the membrane. On the other hand, a thin membrane causes higher diffusion rate of particles such as molecules of hydrogen, water, oxygen, etc., through the membrane. The discribed process is called crossover and usually has a negative effect on the fuel cell operation. It has been intesively studied in relation to direct methanol fuel cell (DMFC), where methanol crossover could cause dramatic losses in performance [19]. Hydrogen crossover effect on the cell performance is not as critical as for DMFC, however, drop in an open cell voltage was observed [20]. Another negative effect linked with hydrogen crossover is membrane degradation caused by local overheating and also by formation of peroxide radicals [21, 22].

With respect to this behavior and potential application a suitable membrane has to be chosen. DuPont company produces a whole series of Nafion membranes, usualy marked by three numbers. First two are related to the equivalent weight, which is defined as the weight of dry membrane per mole sulfonic acid. The last number represents the thickness of membrane in thousandths of inch.

2.3.2 Anode

The anodic side of MEA, which is supplied with hydrogen, is responsible for the hydrogen oxidation reaction (HOR). The overall process described by Eq. (2.3) consists of two steps: dissociative adsorption and oxidation. It can be generally described as follows [23]:

$$\text{Tofel}'\text{sstep}: \ \mathrm{H_2} \ \leftrightarrows \ 2\mathrm{H_{ad}} \tag{2.12}$$

$$\text{Volmer}'\text{sstep}: \ \mathrm{H_{ad}} \ \leftrightarrows \ \mathrm{H^+} \ + \ \mathrm{e^-} \tag{2.13}$$

$$\text{Heyrovsky}'\text{s step}: \ \mathrm{H_2} \ \leftrightarrows \ \mathrm{H_{ad}} \ + \ \mathrm{H^+} \ + \ \mathrm{e^-} \tag{2.14}$$

Anode potential is usually defined with respect to the standard hydrogen electrode (SHE); hence in our case it equals zero by definition.

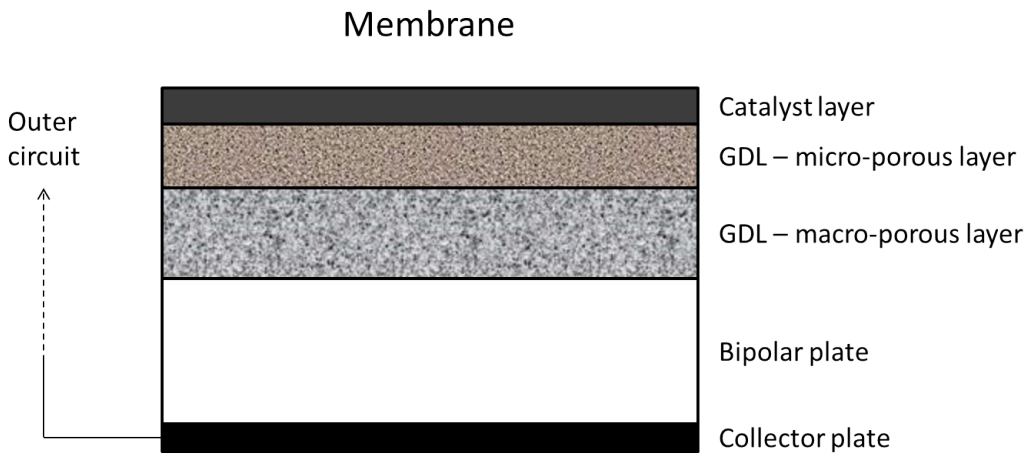

Figure 2.5: Electrode structure

The basic structure of the anode electrode is the same as for the cathode electrode. Both of them consist of several components, each with a specific function during fuel cell operation. Namely, from outside to the membrane, there is a collector plate, a bipolar plate with flow channels, a gas diffusion layer (GDL) or double-layer containing macro-porous and micro-porous layer, and finally a catalyst layer (Fig. 2.5).

Collector plates are made of a metal with current connectors. In contrast to the other electrode components, there are not any special requirements except for a good conductivity.

The same requirement, i.e. a good conductivity, applies also to bipolar plates which have to provide an electrical connection between a catalitically active part of the electrode and the collector plate. However, their main task is to equally supply the whole electrode area with reactant gases. It has been shown that the design of flow channels strongly affects the performance of the cell. One of the best and the most used designs is a serpentine shape [24]. From the material properties, the most important are sufficient strength, impermeability to gases, and chemical stability; [3]. for instance graphite [25] or stainless steel [26] are used.

Even though GDL serves only as a support layer for the catalyst there are strong requirements for its properties. First of all, the reactant gases coming from the bipolar plate have to be able to permeate through the layer to easily reach

the catalytically active sites. This can be achieved by its porous structure and high diffusion coefficient [27]. Further, a good thermal and electron conductivity is required [28, 29]. GDL is also responsible for water removal from the cell. Negative effects of poor water management and electrode flooding were already discussed in the previous chapter and GDL plays a crutial role in their mitigation. There are two ways to affect water transport: first by thermal properties, as it is strongly linked with heat transport [30]. The second possibility is by managing hydrophobic/hydrophilic properties of the layer. This is usually made by adding hydrophobic polytetrafluorethylene (PTFE) or hydrophilic Nafion to the GDL [31]. Multi-layer structures with different wetting properties have been also studied [12].

Carbon cloth or carbon paper with a thickness of a few hundreds of microns represents a typical GDL material. To increase the porosity and thus the surface area, one usually uses a thin micro-porous layer made of carbon powder with an ionomer for ionic conductivity and/or PTFE.

The last layer in a direct contact with the membrane is the catalyst layer. Transition metals, especially of VIII.B group, or their alloys represents typical catalyst material used in proton exchange membrane fuel cells (PEMFC). Although anode and cathode catalyst layers differ in their composition, platinum is considered to be the best catalyst in both cases followed by iridium [23]. Both platinum and iridium, are rare and extremely expensive metals, therefore there is effort to diminish their loading. Commercial catalysts usually contain less than 0.5 mg of platinum per square centimeter [32].

2.3.3 Cathode

The structure of the cathode was thoroughly discussed in the previous section. The process of oxygen reduction reaction is more complicated than the hydrogen oxidation reaction. It consists of several steps, see Fig. 2.6. Maximum efficiency is reached by direct reduction of oxygen to water through four-electrons path marked with reaction rate constant k_1 in Fig 2.6. Incomplete reduction to hydrogen peroxide by two-electrons path leads to a decrease of energy convertion efficiency. Futhermore, hydrogen peroxide can convert to peroxide radicals

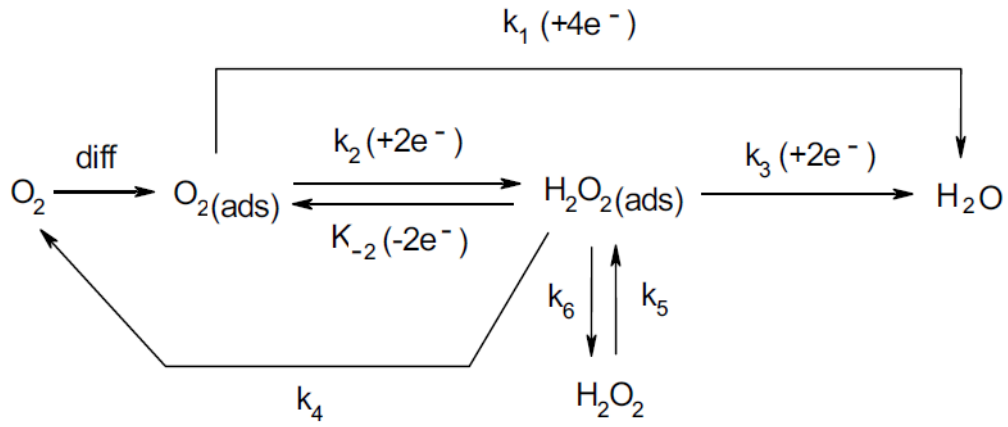

Figure 2.6: Oxygen reduction reaction *(Reprinted from [33])*

causing degradation of the membrane [33].

2.4 Catalyst poisoning

Even though fuel cell technologies have been intensively studied for more than thirty years, and are supposed to be a very promising energy source, there are still difficulties impeding its commercialization. Some of them such as crossover or water management were discussed in the previous sections. However, a high cost of platinum and especially catalyst poisoning are more severe limiting factors as it it leads to the deactivation of catalytically active sites.

2.4.1 CO poisoning

The most discussed compound in the context of catalyst poisoning in fuel cells is carbon monooxide. The harmful effect of its presence in fuel on the cell performence is well known since the 90s. It was shown [2] that Gibbs free energy of adsorption on platinum is comparable for hydrogen and CO ($\approx -55\,\mathrm{kJ/mol}$) at temperature higher than 100 °C [34]. However, at lower temperatures, which are typically used in fuel cell, the Gibbs free energy of adsorption of CO is lower (more negative) which in turn leads to preferential adsorption of CO on platinum. It was estimated [2] that the sticking probability on platinum is fifteen times higher for CO than for hydrogen. Linearly or bridge-bonded CO molecules block platinum sites for hydrogen dissociative adsorption and oxidation (Eq. (2.12) - (2.14)).

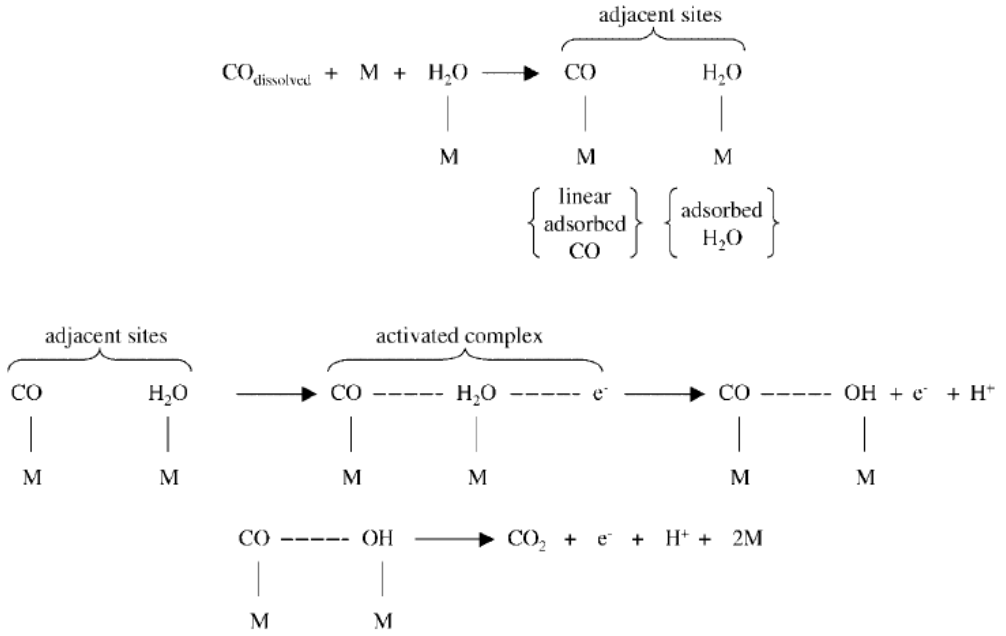

Figure 2.7: CO oxidation on a metal adsorption site (M) (*Reprinted from [2]*)

The decrease of current shows quadratic dependence density with increasing CO coverage [2]

$$i(\theta_{CO}) = i_0(1 - \theta_{CO})^2, \tag{2.15}$$

where i_0 is current density with pure hydrogen fuel and zero CO coverage. Tofel's step (2.12) of hydrogen oxidation offers the best explanation for quadratic decrease. Dissociative adsorption requires two adjacent platinum sites. Thus the adsorbed CO molecule, in addition to blocking the platinum site, also decreases the probability of a participation of the surrounding sites in the reaction. The given explanation is purely intuitive as any serious model studying this problematic has not been proposed yet.

Carbon monooxide is strongly bonded to platinum. Its oxidation potential, $0.6-0.8\,\mathrm{V}$, is much higher than $0-0.2\,\mathrm{V}$ for hydrogen oxidation [35, 36]. Furthermore, CO oxidation rate decreases with CO coverage because the process requires two adjacent sites (Fig. 2.7). These obseravations result in a strong sensitivity to the CO presence in the fuel, and even a small amount of it in the range of tens of ppm could have a significant effect on the fuel cell performance [37]. Aside from the CO concentration, the poisoning effect is affected by temperature and pressure. However, the pressure dependance is relatively weak [38].

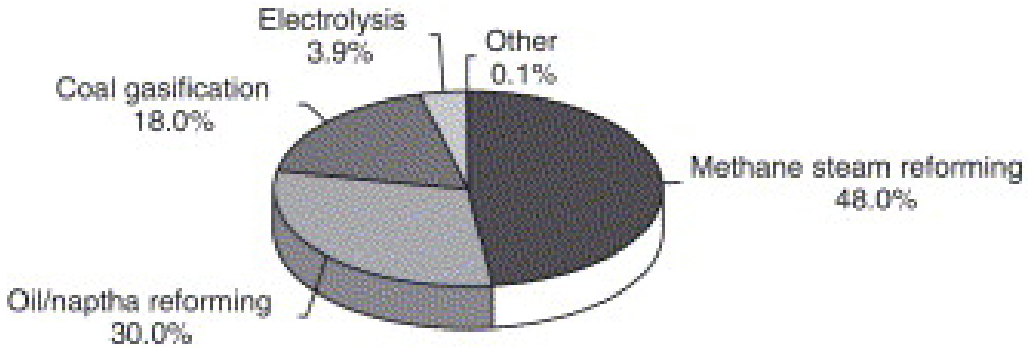

Figure 2.8: Worldwide production of hydrogen (*Reprinted from [40]*)

2.4.2 Sources of CO in the fuel

For useability of fuel cells as a widespread energy source low cost of hydrogen is crucial. The most suitable way of hydrogen production for fuel cell applications is electrolysis. In this case, the fuel is clean and contains almost no contaminants. Unfortunately, electrolysis is one of the most expensive ways of mass production of hydrogen. The cost of a centralized production in US is approximately 1.5 - 2 times higher than for other techniques and for distributed production even 4 times higher [39]. There is a tendancy to decrease the electrolysis cost, but according to current progress, it would not reach the cost of other techniques in less than 30 years. Nowadays, electrolysis represents only $3 - 4\,\%$ of worldwide hydrogen production and over $96\,\%$ of hydrogen is made from fossil fuels [1]. Reformation of natural gas, especially methane, or oil plays a dominant role. Coal gasification - propeling of water vapour through coal at high pressure and temperature - is also commonly used. Comparison of different techniques is given in Fig. 2.8. In all these methods, the produced hydrogen is rich i carbon-based contaminants such as carbon monooxide, carbon dioxide or methane.

2.4.3 Possibilities of CO tolerance enhancement

With respect to the previous part, contaminants are present in the fuel and fuel cell stability under these conditions is a crucial question. There are three main ways how to enhance the durability of a fuel cell and its tolerance against CO poisoning: increase of the operating temperature, addition of a small amount of oxygen to the fuel, the use of alloys of platinum and other metals as a catalyst.

It was found that the effect of CO poisoning depends on temperature. High temperature helps to reduce the CO coverage by promoting its oxidation [41]. However, operating temperatures higher than the standardly used $80-100\,^{\circ}\mathrm{C}$ are problematic. They are not practical for applicationsand we encounter problems with membrane stability, as the glass transition point of Nafion lies in the range of $110-120\,^{\circ}\mathrm{C}$.

The second possibility, known as air- or oxygen-bleeding, is based on injection of a small amount of oxidant into the anode gas stream. It was experimentally shown that less than $2-5\,\%$ of oxygen could eliminate the harmful effect of CO up to concentrations in order of a few hundreds of ppm [42]. However, the disadvantege of oxygen-bleeding is a decrease in the conversion efficiency caused by a direct reaction of the introduced oxygen with hydrogen. A theoretical study of oxygen crossover through the membrane [43] shows that oxygen flux into the anode, assuming Nafion 117, is approximately $1\,\%$ of hydrogen flux which is relatively close to the optimal interval of oxygen-bleeding found experimetally.

The third option is using alloys of platinum with another metal, most commonly ruthenium, as an anodic catalyst. The presence of ruthenium decrease oxidation potential of CO by almost $200\,\mathrm{mV}$ [44]. Furthermore, water adsorbs preferentially on ruthenium, creating Ru-OH group, which in turn leads to an easier oxidation of CO adsorbed on an adjacent platinum site [2]. Another alloys, usually platinum with a d-metal, such as PtCo, PtNi, PtPd, PtMo etc., have been also studied; however, PtRu lead to the best results [45].

3. Experimental

This thesis focuses on the anodic side of fuel cell, hydrogen oxidation reaction and the effect of contaminants in the fuel. MEA was made of a commercial cathode and an anode prepared by magnetron sputtering. Nafion 117 was used as a membrane for all samples.

3.1 Magnetron sputtering

Magnetron sputtering represents a deposition technique of surface physics. It is usually used for the preparation of thin layers with thickness from a few nanometers up to a few microns.

The basic principle is as follows. The cathode, also called target, which is a disc made of the demanding material, is bombared by highly energetic ions produced by plasma discharge glow. As the ions collide with the target, atoms or whole clusters are removed from the material and "fall" on the substrate where they condense and create a thin film.

The whole process occurs in a vacuum with pressure less than 1 Pa. To ensure the required purity of residual atmosphere, the deposition chamber is purged down to 10^{-4} Pa and then filled with inert gas, usually argon. Atoms of argon are ionized by collisions with electrons accelerated by an external electic field. Argon ions Ar^+ are hitting the target where thez initiate collision cascades between the target atoms, which in turn results in their transfer to the gas phase and possible condensation on a sample placed in front of the target.

This sputtering process is limited by relatively low deposition speed, and a necessity of high voltage applied. To overcome these disadvatages, an external magnetic field perpendicular to the surface is applied, see Fig. 3.1. The magnetic field curves the trajectories of the electrons, which leads to their prolongation and a significant increase in ionization probability, and consequently to a higher deposition speed. A source of direct current is standardly used for the deposition of conductive materials. To deposit an insulator, such as ceramics, a radio frequency source is required.

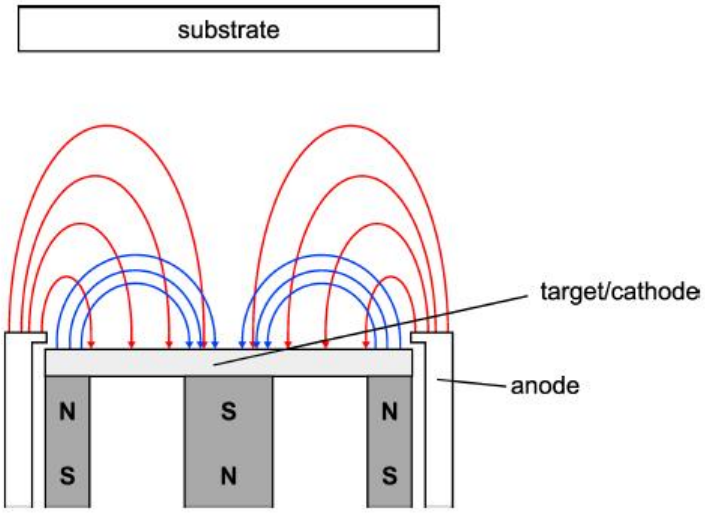

Figure 3.1: A schematic drawing of magnetron. Electric and magnetic fields are indicated by red and blue lines, respectively. *Reprinted from [46]*

As alluded to, the atmosphere in the chamber is constituted by argon or another inert gas. To prepare thin films of basic compounds, such as oxides or nitrides, reactive magnetron sputtering could be used. During this process, a small amount of oxygen or nitrogen (in order of tenths of percent) is added to argon. Released atoms or clusters of the target react with the gases and form the required layer.

The deposition of a catalyst on etched Nafion membranes was achieved using a method developed at our departement. It consists of etching membrane by ionic plasma and a subsequent deposition of a thin ($\approx 1 - 10\,\mathrm{nm}$) layer of CeO_2. The pre-treatment results in a structure with high porosity, as can be seen in the Fig. 3.2. All etched membranes used in this thesis were prepared by Yurii Yakovlev.

The magnetron available at our departement consists of three heads places symmetrically with respect to the sample (Fig. 3.3) allowing simoultaneous deposition of three different materials. Both platinum and ruthenium are good conductors, hence DC mode was used for the deposition. The deposition speed was regulated by controlling the power of the DC source. Parameters of the deposition are summarized in Tab. 3.1. To estimate the Pt loading, previous calibration done at out departement, and a linear dependence between power and deposition speed were assumed.

a) 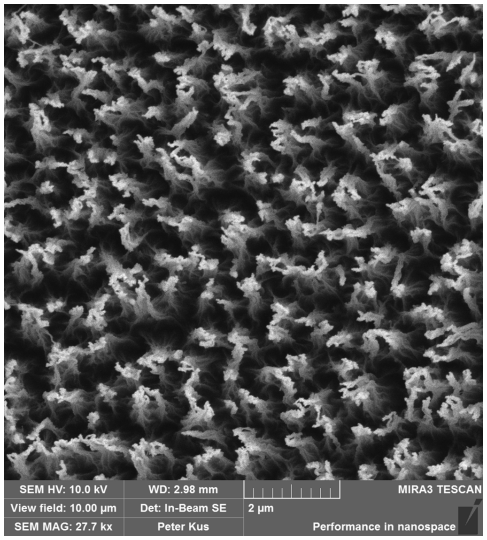

b) 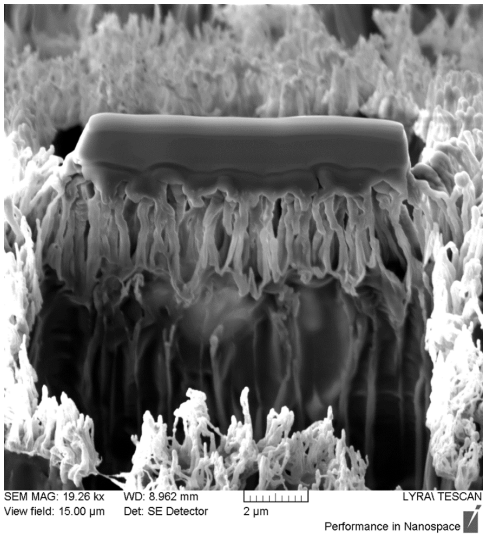

Figure 3.2: SEM images of etched Nafion membrane with CeO_2 layer. a) Top view Nafion 117 b) Cross-section Nafion NR212 *(The images were made by Peter Kus and Jaroslava Lavkova)*

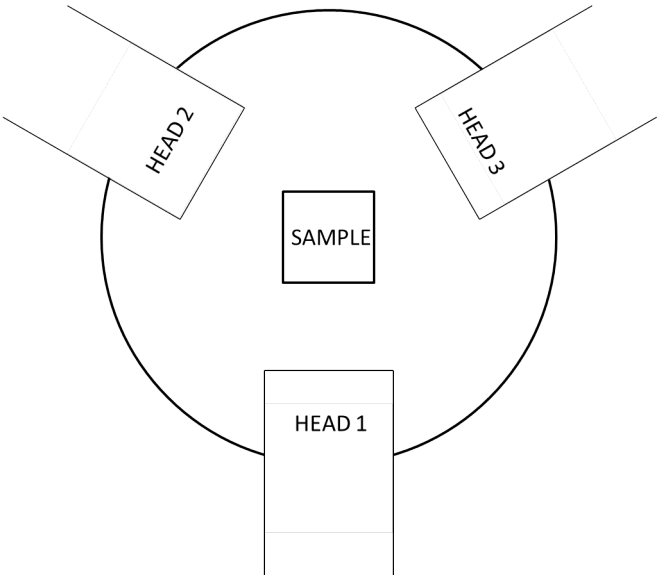

Figure 3.3: Scheme of a magnetron

Sample	Power Pt [W]	Power Ru [W]	Time [s]	Pt loading [μg/cm^2]
Pt	20	0	510	30
PtRu 1:1	20	30	510	30
PtRu 2:1	20	15	510	30
PtRu 1:2	20	60	510	30

Table 3.1: Magnetron sputtering - deposition parameters. The ratio in the first column represents atomic ratio between Pt and Ru. *(First two sample were prepared by Yurii Yakovlev.)*

3.2 Testing station

All measurements were carried out *in operando* under real operating conditions. A piston cell from GreenLight Innovation was used. The piston pressure and operating temperature were held constant during the whole experiment at 8 bar and 70 °C, respectively. Temperature of bubblers in hydrogen and nitrogen lines were set to 70 °C, and in oxygen line it was 65 °C, which results in relative humidity of 100 % at the anode. It is difficult to determine relative humidity at the cathode due to the production of water. An appropriate estimation might be $80 - 100$ %.

A simplified scheme of the station is shown in Fig. 3.4. Pure hydrogen and oxygen from AirLiquid were used as a fuel and oxidizing agent, respectively. Gas flow was set to 80 sccm at the anode and 64 sccm at the cathode. Both of them were humidified in the bubbler prior to entering the cell. The pressure inside the cell was maintained between 0.2 bar and 0.5 bar by two back pressure regulators, one for each line. Three-way valves in hydrogen and oxygen lines served to cleaning the system before and after opening the cell.

For the purposes of this thesis, a new panel for mixing of the gases was constructed. Two-step mixing was used in order to reach sufficiently low concentration of CO required for the poisoning study with a good accuracy. Initial gases were pure hydrogen and a calibrated mixture of 1 % CO in hydrogen. The whole hydrogen line with the mixing panel is shown in Fig. 3.5. Originally a difference of two orders of magnitude between the flows in FC1 and FC2 lead to an instability in FC1 flow, thus the check valve CV1 was added, it serves only for the

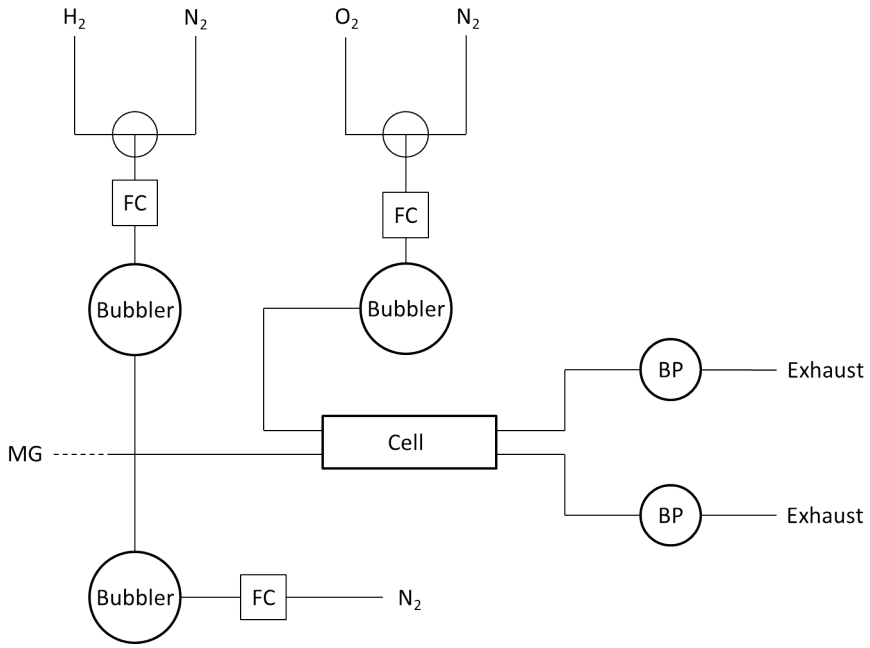

Figure 3.4: Simplified scheme of testing station. FC - Flow controller, BP - Back pressure regulator, MG - Mixture of gases for poisoning measurements

Flow controller	Range [sccm]	Accuracy
FC1	0-5	$0.8\% + 0.01$ sccm
FC2	0-500	$0.8\% + 1$ sccm
FC3	0-100	$0.8\% + 0.2$ sccm
FC4	0-100	$0.8\% + 0.2$ sccm
FC5	0-500	$0.8\% + 1$ sccm

Table 3.2: Technical parameters of flow controllers

stabilization of the first mixing step. A part of the mixture from the first step is used in the second step and the rest is taken away by CV2 into exhaust. There is not any bubbler in the mixing pannel and thus none of the gases is humidified. This is not crucial as the output of FC3 creates at most 10 % of the total gas stream injected into the cell.

Alicat Precision Gas Mass Flow Controllers from MC-series were used. Technical parameters are listed in Tab. 3.2. This particular type of controllers allows for concentrations as low as 5 ppm, which was also achieved with accuracy ± 0.4 ppm.

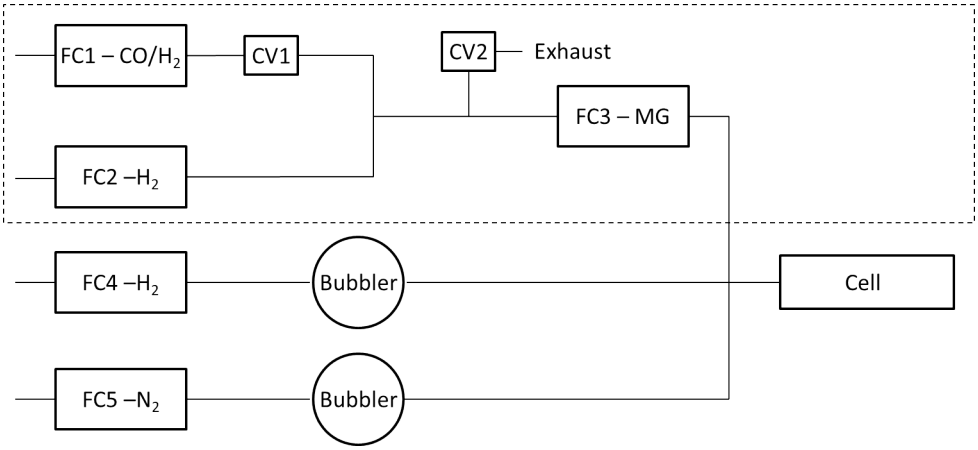

Figure 3.5: Scheme of mixing panel in dashed rectangle, the rest is corresponding to hydrogen and nitrogen lines in Fig. 3.4. FC - flow controller, CV - check valve

To study the effect of catalyst poison on fuel cell performance, a constant voltage of 650 mV was held and a power response to different CO or N_2 was observed. Voltage and current were measured by a four-probe method using Programmable DC Electronic Load BK Precision 8500. Five different phenomena were studied.

(1) Effect of fuel dilution by nitrogen - ratio between nitrogen and hydrogen was changed holding the total flow of the mixture constant.

(2) Effect of partial pressure of hydrogen - in this case, hydrogen flow was held constant and different amount of nitrogen was added to the fuel.

(3) CO poisoning - a small concentration of CO from 5 ppm up to 250 ppm was added to hydrogen.

(4) Effect of CO partial pressure - hydrogen and CO flow was held constant and nitrogen was added to the mixture.

(5) Combined effect of CO and nitrogen - hydrogen flow was constant and nitrogen was added ajusting the CO flow to hold constant CO concentration in the whole mixture.

To set a new sample into operation so-called “break-in procedure” was done. It consists of a set of IV curves, periods of constant voltage or current, which

lasts in total approximately $20 - 24$ hours. The main goal of this procedure is moisturisation of the membrane and stabilization of the fuel cell.

4. Results

In total, eight samples were studied. In all cases, commercial cathode with platinum content of 0.3 mg/cm^2 or 0.5 mg/cm^2, Nafion 117 and GDL with microporous layer as a support at the anodic side were used. All samples differentiated by anode catalyst are listed in Tab. 4.1.

Sample	Anode	Cathode
Reference	commercial 0.3 mg/cm^2	commercial 0.5 mg/cm^2
Pt105	Pt	commercial 0.5 mg/cm^2
PtRu115	PtRu 1:1	commercial 0.5 mg/cm^2
PtRu215	PtRu 2:1	commercial 0.5 mg/cm^2
PtRu125	PtRu 1:2	commercial 0.5 mg/cm^2
Pt103	Pt	commercial 0.3 mg/cm^2
PtRu113	PtRu 1:1	commercial 0.3 mg/cm^2
PtRu123	PtRu 1:2	commercial 0.3 mg/cm^2

Table 4.1: List of samples. Deposition parameters of anodes are listed in Tab. 3.1. The sample name is based on its composition, first two digits represents the ratio between platinum and ruthenium, and the last one denotes the type of the cathode.

4.1 The reference sample

A commercial anode with platinum content of 0.3 mg/cm^2 was used to prove the concept of gas mixing and to have a referential point to compare with other samples . The sample showed a relatively good stability and performance. Maximum power after break-in was 3 965 mW at 550 mV, which, assuming electrode area 4.4 cm^2, results in power density 900 mW/cm^2 and specific power 1 124 mW/mgPt.

Fig. 4.1 shows the hydrogen dilution effect. The total flow was held constant at 80 sccm and the ratio between nitrogen and hydrogen was changed from 50 % of nitrogen up to 80 %. Between each two nitrogen exposures, pure hydrogen was injected into the cell for some time for the sample to recover and stabilize. In the

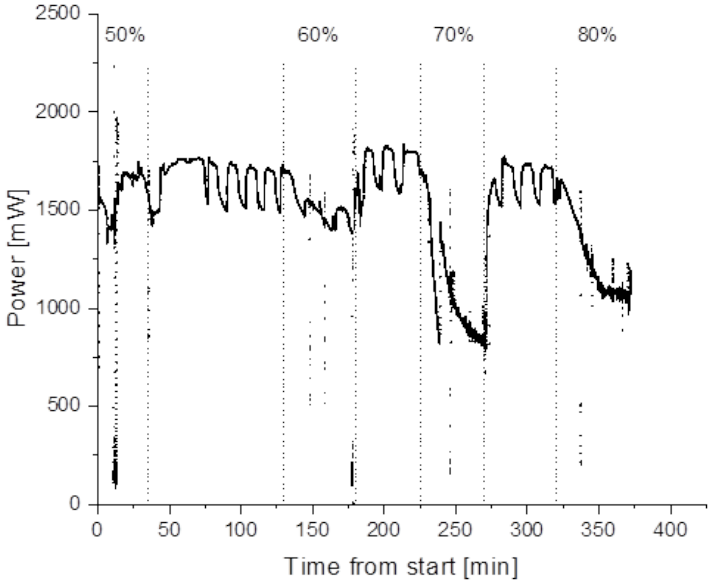

Figure 4.1: Reference - Effect of hydrogen dilution with 50 %−80 % of nitrogen. In the gaps between each two intervals of exposure to contaminants, pure hydrogen was used to restore the initial value of power.

case of low nitrogen concentration, a decrease in the power was slightly higher than 10 %. In the case of higher concentration, the lack of hydrogen becomes more evident and a decrease in power reaches tens of percent. Oscillations with a period of approximately 15 min can be also seen in Fig. 4.1. This type of behavior was observed for all samples. The most probable cause is water condensation in the serpentine shaped flow field or catalyst surface, which blocks the hydrogen input. Different mass flow from 80 sccm up to 200 sccm at the anode did not affect the oscillations. Similar behaviour was observed in a previous work done at our department [47].

On the other hand, the performance of the system changed only very little with different partial pressures of hydrogen (Fig. 4.2). In this case, hydrogen flow was set to 80 sccm and additional nitrogen was injected into the system to reach the required concetration. Apart from the oscillations explained above, no changes in the cell performance were observed.

CO poisoning was measured in the concentration range $5 - 250$ ppm. The sample showed strong dependence on the CO presence. Fig. 4.3 shows that even

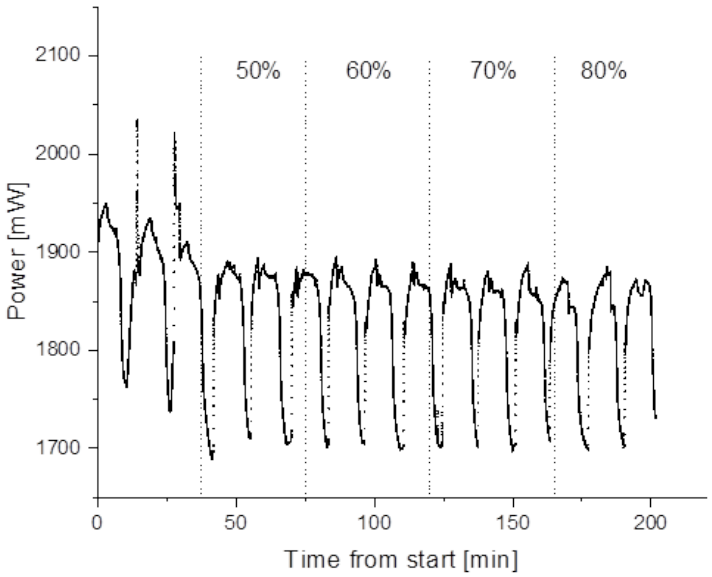

Figure 4.2: Reference - effect of hydrogen partial pressure. Nitrogen concetration was changed from 50 % to 80 %. In the gaps between each two intervals of exposure to contaminants, pure hydrogen was used to restore the initial value of power.

for CO concentration as small as 25 ppm, the drop in power represents 90 % of its initial value. For concentrations higher than 50 ppm, the power barely reached 5 % of the initial value, see Fig. 4.3). Thus threshold of CO poisoning lies between 25 ppm and 50 ppm. The recovery of the catalyst after disconnection of CO was extremely fast. The power was restored in a few tens of seconds. Time intervals between two CO cycles were in the order of minutes.

The effect of simoultaneous decrease of partial pressure of hydrogen and CO was studied next. The total flow of the mixture - 10 ppm of CO in hydrogen - was held constant at 80 sccm and different amounts of nitrogen were added similarly as in the second discussed case. Thus the CO concetration in the total flow changed depending on the nitrogen flow. An increase in nitrogen concentration results in a decrease of CO partial pressure, which should lead to an increase in power. However, Fig. 4.4 shows that this increase is hardly observable. This might be explained by the fact that the ratio between CO and hydrogen is constant and it is probably more significant than CO partial pressure.

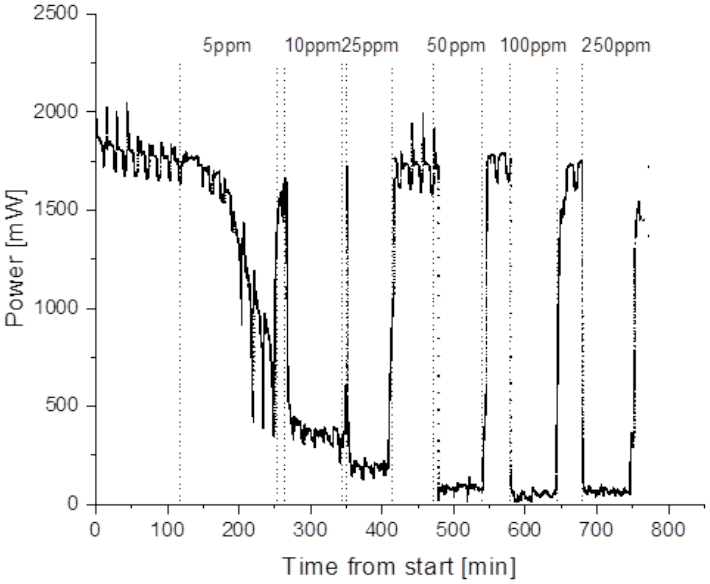

Figure 4.3: Reference - CO poisoning for concetration from 5 ppm to 250 ppm. In the gaps between each two intervals of exposure to contaminants, pure hydrogen was used to restore the initial value of power.

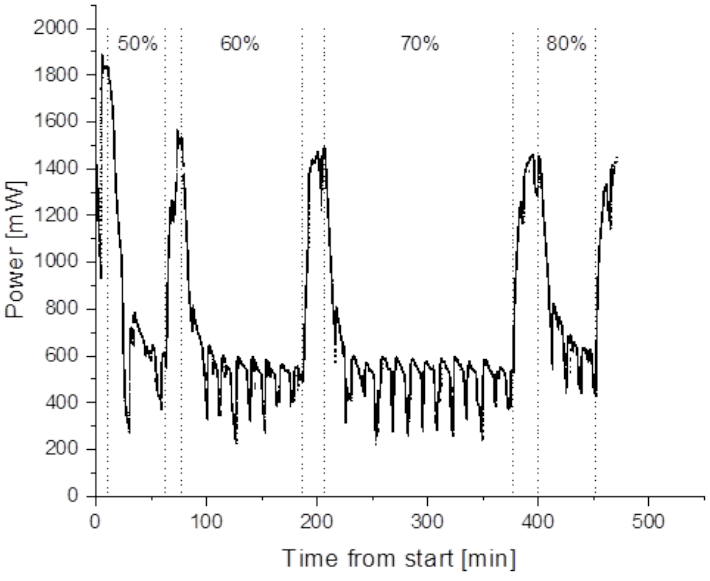

Figure 4.4: Reference - Effect of simoultaneous decrese of CO and H_2 partial pressure. Individual regions represents different nitrogen concentrations. In the gaps between each two intervals of exposure to contaminants, pure hydrogen was used to restore the initial value of power.

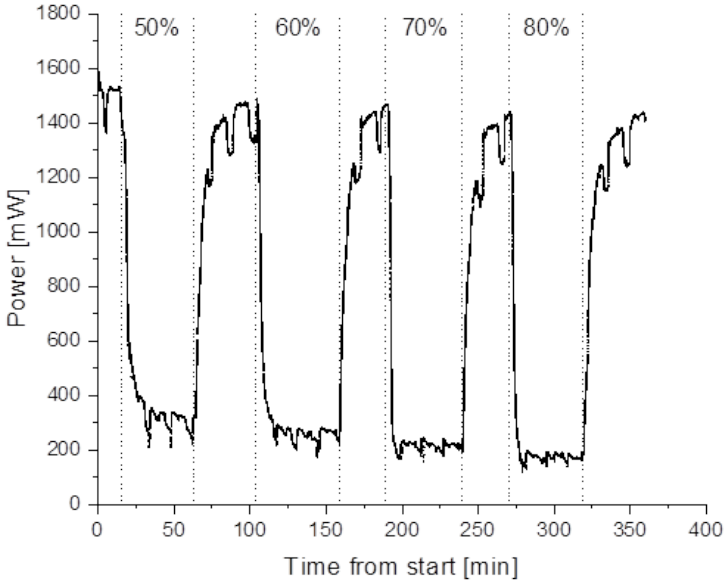

Figure 4.5: Reference - Combined effect of 5 ppm of CO and nitrogen with concentration from 50 % to 80 %. In the gaps between each two intervals of exposure to contaminants, pure hydrogen was used to restore the initial value of power.

If the CO flow was increased proportionally to the nitrogen flow, i.e. to hold CO concentration constant at 10 ppm given the whole mixture, effects of CO poisoning and hydrogen partial pressure decrease combined, and lead to a higher drop in power (Fig. 4.5) than one would expect separetely for each of these phenomena. The hydrogen flow was again 80 sccm and the ratio of CO and hydrogen increased which could explain decrease in the power.

4.2 Pure platinum

The same set of experiments was carried out for a catalyst layer of pure platinum sputtered directly on an etched membrane. The platinum loading was 30 μg/cm^2 which is ten times lower than the loading of a commercial one. Two different commercial cathodes were used.

The maximum power after break-in was 2 295 mW for Pt103 and 2 442 mW for Pt105 which is approximately 60 % of the reference value. On the other

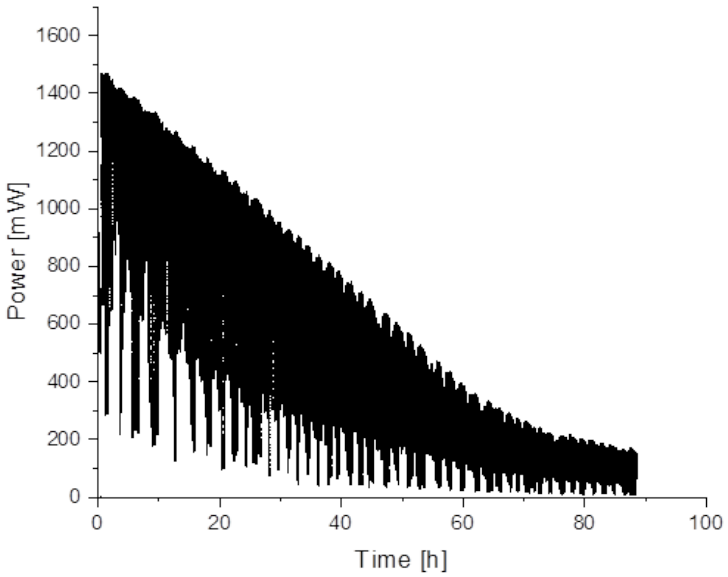

Figure 4.6: Pt103 - Degradation of the sample during the time. Time zero represents the end of first nitrogen experiment (approximately 2 days after break-in). Voltage was held at 650 mV.

hand, specific power 1 577 mW/mgPt and 1 045 mW/mgPt was comperable or even higher than the reference 1 124 mW/mgPt.

Sample Pt103 showed longterm instability, and after the first experiment with nitrogen (similar to Fig. 4.1 - nitrogen concentration between 50 % and 80 % and a constant total flow), the sample began to degrade (Fig. 4.6). During the four days when it was supplied only with pure hydrogen, i.e. without nitrogen or CO, it lost almost 90 % of its performance.

Sample Pt105 was more stable and experiments with nitrogen could be carried out. As was the case of the reference, the sample did not react to the changes of partial pressure of hydrogen. Constant hydrogen flow of 80 sccm and changes in the nitrogen flow did not lead to any observable reaction.

On the other hand, the effect of hydrogen dilution was more significant. Similarly to Fig. 4.1, the total flow was held constant and the ratio between hydrogen and nitrogen was changed. Fig. 4.7 shows that for nitrogen concentration of 80 % the power drop was around 70 % of its initial values.

We also observed that the presence of CO in the fuel had the devastating

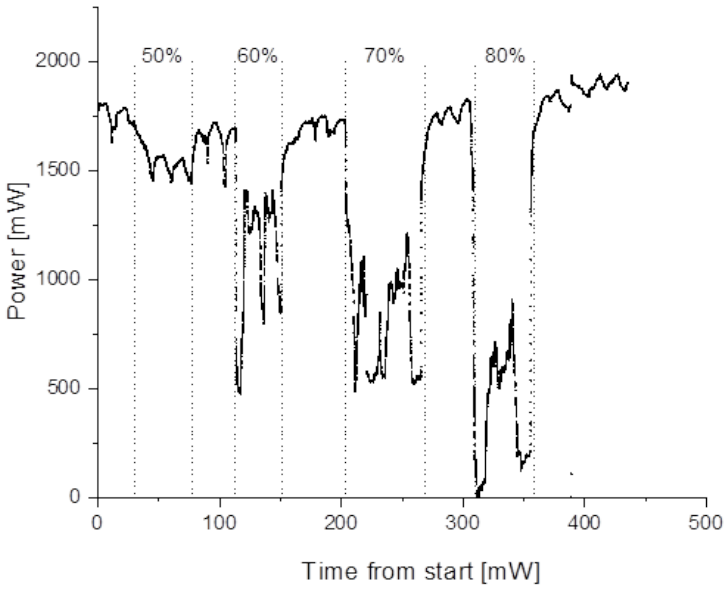

Figure 4.7: Pt105 - Effect of hydrogen dilution with 50 %-80 % of nitrogen. In the gaps between each two intervals of exposure to contaminants, pure hydrogen was used to restore the initial value of power.

effect on the performance of fuel cell. Even for the lowest CO concentration of 5 ppm, the power fell down to 1 % of its initial value. The recovery time after ending of CO exposure increased, see Fig. 4.8. The delay between the end of the exposure and an increase in the power was in the order of minutes for 10 ppm of CO instead of few second observed for the reference. To complete the recovery, a cyclic voltammetry between 0.05 V and 1.15 V had to be done, otherwise one could not proceed with the experiment. The electrochemical cleaning of the surface had an extremely beneficial effect. The maximum power grew from 2 442 mW after break-in to 3 867 mW at 520 mV which is comparable with the reference.

Interesting results were obtained for a combined exposure to nitrogen and CO. If the total flow of mixture of 5 ppm of CO in hydrogen was held constant and additional nitrogen was added, the decrease in CO partial pressure caused a significant increase in power from 800 mW at 50 % of nitrogen up to 2 000 mW at 80 % (Fig. 4.9). This increase disagrees with the hypothesis that the effect of the ratio of CO and hydrogen is more significant than CO partial pressure. On the other hand, CO concentration of 5 ppm is higher than the threshold of poisoning,

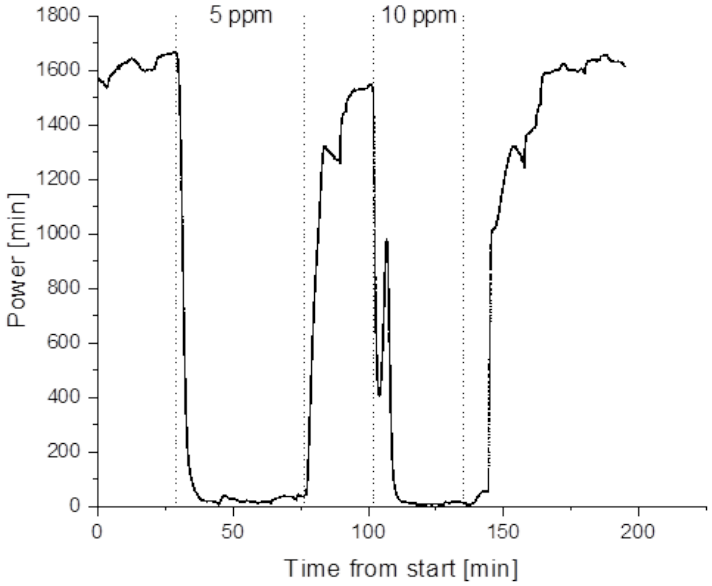

Figure 4.8: Pt105 - CO poisoning. In the gaps between two intervals of exposure to contaminants, pure hydrogen was used to restore the initial value of power.

which might explain the different behavior.

The second experiment with constant hydrogen flow 80 sccm, CO concentration of 5 ppm (given the whole mixture), and different additional nitrogen flow also lead to a stronger dependence than in the case of reference. Nitrogen concentration was changed from 50 % to 80 %. The initial value of the power, the same as in previous case, was significantly higher than during CO poisoning. This was most probably caused by a cyclic voltammetry done prior to these experiments. However, for high nitrogen concentrations ($70 - 80$ %) the power fell down again to the values lower than 1 % of the initial value. It is also interesting to observe a prolongation of recovery time with increasing nitrogen concentration from few seconds at 50 % up to few minutes at 80 % of nitrogen.

4.3 Platinum-ruthenium

As already mentioned, using PtRu alloys could be a viable way to enhance the CO tolerance of the catalyst. The question of PtRu ratio has been studied, however, with no conclusive results. Nowadays, 1:1 ratio is supposed to be the best [45].

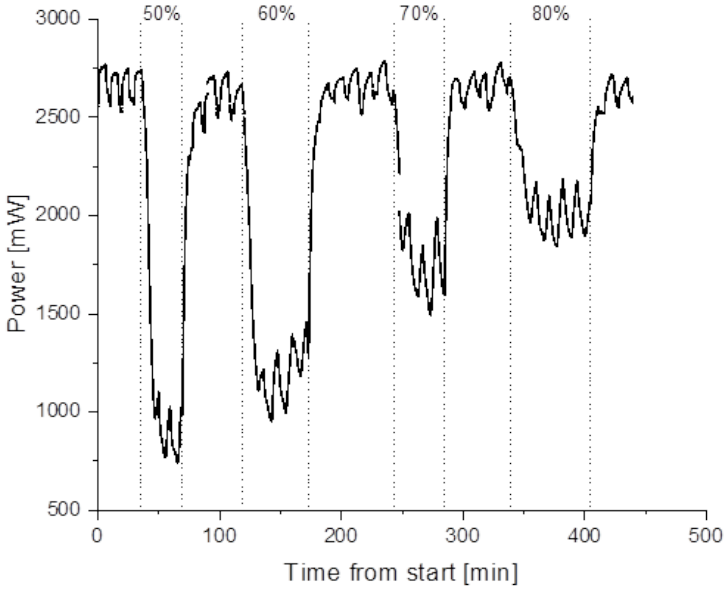

Figure 4.9: Pt105 - Effect of simultaneous decrease of CO and H_2 partial pressure with $50\,\% - 80\,\%$ of nitrogen. In the gaps between each two intervals of exposure to contaminants, pure hydrogen was used to restore the initial value of power.

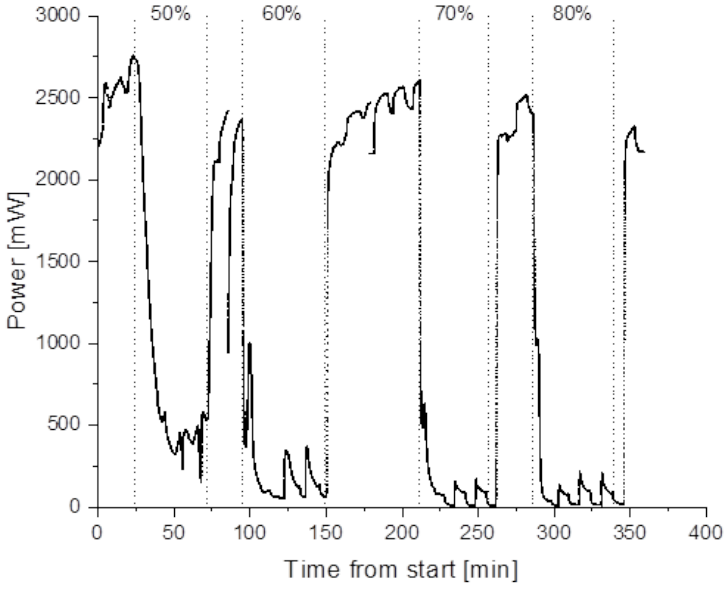

Figure 4.10: Pt105 - Combined effect of 5 ppm of CO and nitrogen with concentration from 50% to 80%. In the gaps between each two intervals of exposure to contaminants, pure hydrogen was used to restore initial value of power.

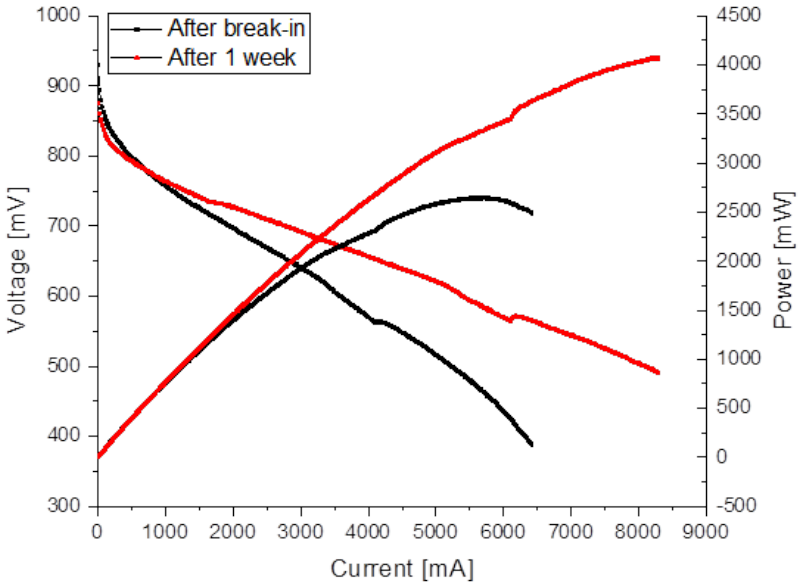

Figure 4.11: PtRu115 - Comparison of IV curves after break-in and after one week

In this thesis, three different ratia 2:1 (PtRu215), 1:1 (PtRu113 and PtRu115) and 1:2 (PtRu123 and PtRu125) were studied.

4.3.1 PtRu 1:1

PtRu113 demonstrated exactly the same stability problem as sample Pt103. Approximately two day after break-in it began to degrade. The changes were reversible, and it was possible to restore the power using cyclic voltammetry. However, it began to degrade again in a short period of time (several hours) regardless of the treatment done meanwhile.

The maximum power of PtRu115 after break-in was 2 644 mW, but it was growing over time without cyclic voltammetry up to 4 072 mW (Fig. 4.11 which is even higher than for the reference. The results for nitrogen experiments were almost the same as for Pt105. More than a 70 % drop of power was observed for hydrogen diluted with 80 % of nitrogen (Fig. 4.12). The only difference with respect to Pt105 was better stability or lower amplidute of oscillation. There was again no reaction to changes of hydrogen partial pressure as it was the case of all previous samples.

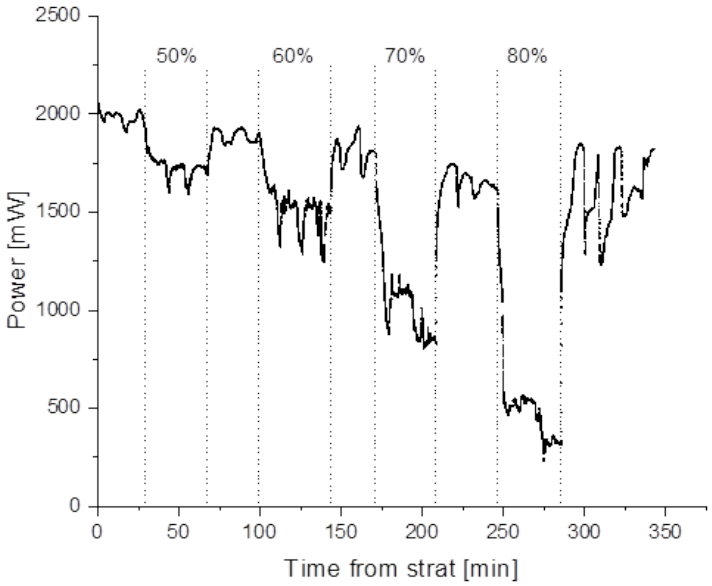

Figure 4.12: PtRu115 - Hydrogen dilution with $50 - 80\,\%$ of nitrogen. In the gaps between each two intervals of exposure to contaminants, pure hydrogen was used to restore the initial value of power.

Fig. 4.13 shows that, in comparison with Pt105, the devastating effect of CO poisoning was partially suppressed for CO concetration of 5 ppm, but 10 ppm had exactly the same devastating effect. The atalyst recovered relatively fast by itself. However, it never reached again the initial value of power, not even after cyclic voltammetry. A sudden drop during the recovery between 5 ppm and 10 ppm was caused by a short-time lost of contact.

The reaction to a combined exposure to nitrogen and CO was similar to the reference. There was a barely measureable increase in power with decreasing CO partial pressure (Fig. 4.14), and no observable reaction to increasing nitrogen and constant CO concentration (Fig. 4.15). In both cases, the maximum power after exposure and recovery decreased, however, it was more significant in the former case. In addition, instability and amplitutde of oscillation increased.

4.3.2 PtRu 2:1

Maximum power 2 866 mW after break-in of PtRu215 was the highest of all sputtered samples. The behavior of the sample during hydrogen dilution was in

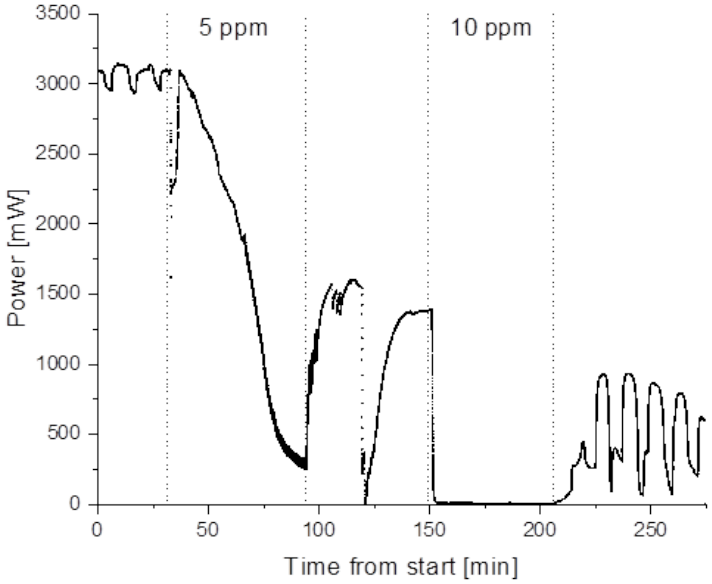

Figure 4.13: PtRu115 - CO poisoning for CO concetrations of 5 ppm and 10 ppm. In the gap between two intervals of exposure to contaminants, pure hydrogen was used to restore the initial value of power.

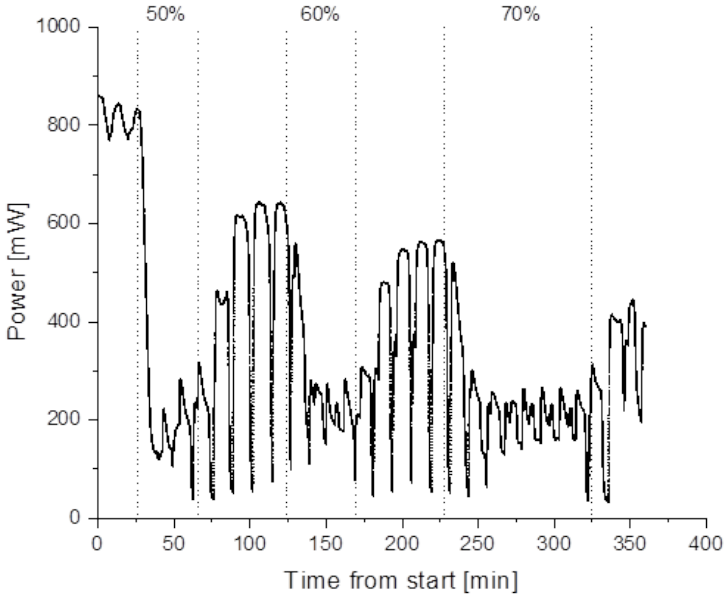

Figure 4.14: PtRu115 - Simoultaneous decrese of CO and hydrogen partial pressure. Nitrogen concetration goes from 50 % to 70 %, 5 ppm of CO with respect to hydrogen. In the gaps between each two intervals of exposure to contaminants, pure hydrogen was used to restore the initial value of power.

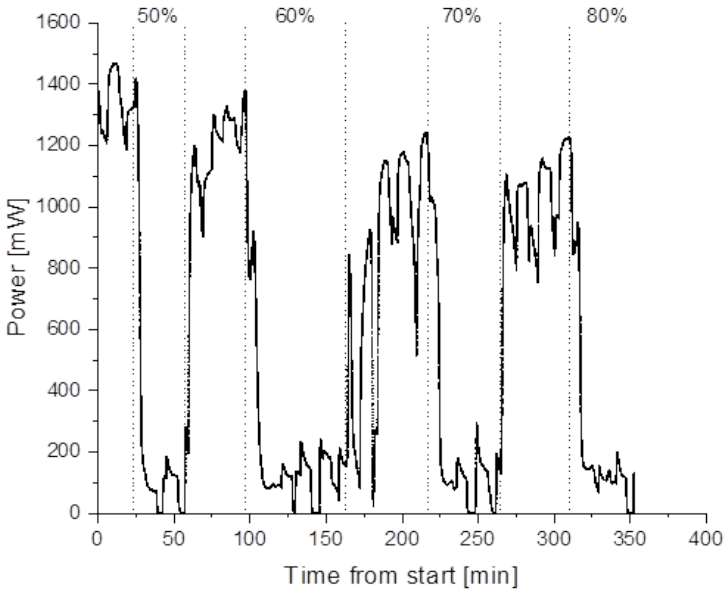

Figure 4.15: PtRu115 - Combined effect of 5 ppm of CO and nitrogen with concentration from 50 % to 80 %. In the gaps between each two intervals of exposure to contaminants, pure hydrogen was used to restore the initial value of power.

general similar to previous samples. However, some kind of instability which can not be easily explained was observed (Fig. 4.16). Instead of standard oscillations sudden step changes appeared. Even though the behavior was different with respect to previous samples, the period of these instabilities was same as period of the oscillations. Furthermore, they diminished during further experiments.

Despite these instabilities, it showed the best CO tolerence of all sputtered samples (Fig. 4.17). The drop in power is still dramatical, but it is not as devastating as for the other samples. Furthermore, the recovery time is extremely short and even after exposure of 50 ppm of CO, the sample reached the initial value of power by itself without cyclic voltammetry.

Unfortunately, the combined effect of CO and nitrogen could not be measured due to unexpected laboratory error resulting in a longterm exposure of the sample to the atmosphere and mixing of oxygen and hydrogen at the electrodes. This had devastating and irreversible effect on the sample.

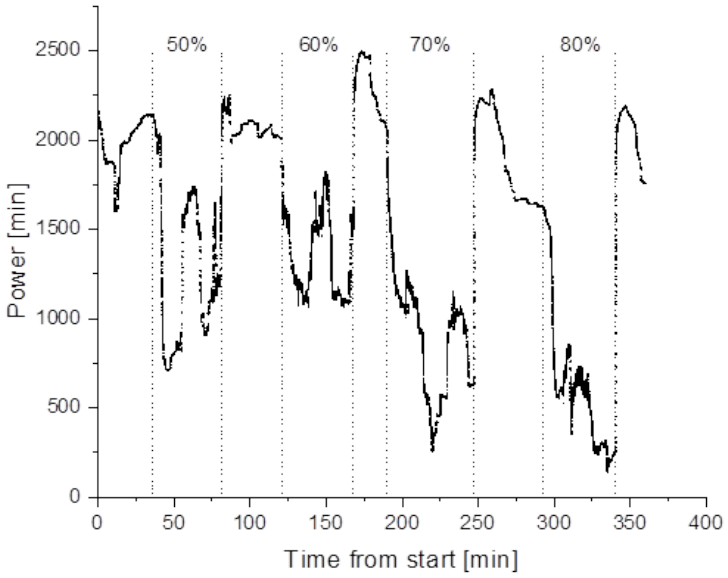

Figure 4.16: PtRu215 - Hydrogen dilution with $50 - 80\,\%$ of nitrogen. In the gaps between each two intervals of exposure to contaminants, pure hydrogen was used to restore the initial value of power.

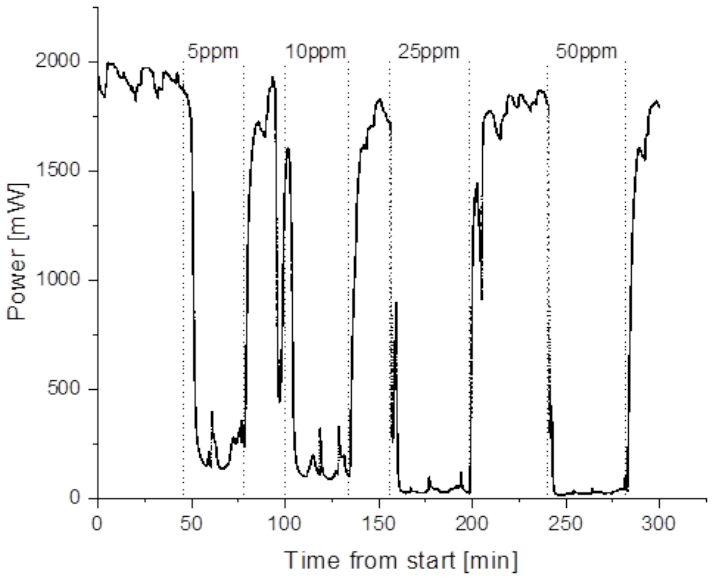

Figure 4.17: PtRu215 - CO poisoning with concentrations from 5 ppm to 50 ppm. In the gaps between each two intervals of exposure to contaminants, pure hydrogen was used to restore the initial value of power.

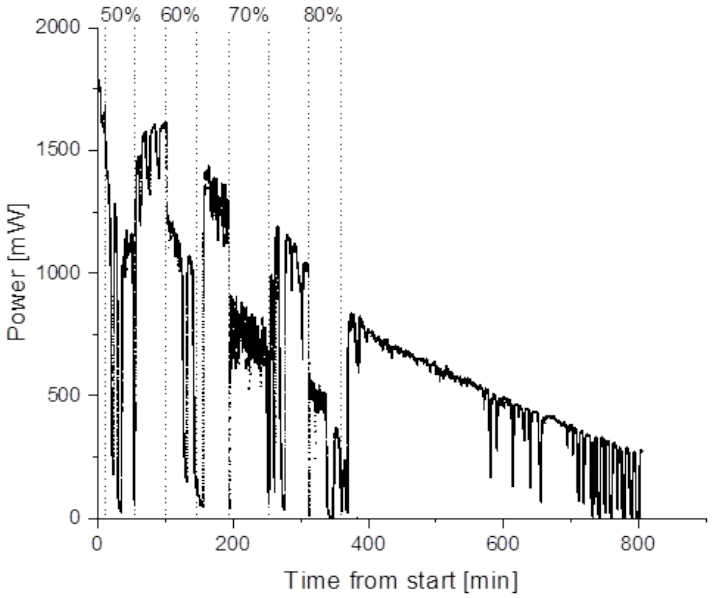

Figure 4.18: PtRu125 - Effect of hydrogen dilution with $50-80\,\%$ of nitrogen and degradation of the sample. In the gaps between each two intervals of exposure to contaminants, pure hydrogen was used to restore the initial value of power.

4.3.3 PtRu 1:2

Last set of measurements was done with platinum-ruthenium ratio 1:2. The results show that the excess of ruthenium is not beneficial and it is even counterproductive. Both samples, irrespective of the cathode type, showed low performance and stability, and both samples started to degrade quickly (appreximately after two days). Maximum power after break-in was 1 265 mW and 2 127 mW for PtRu213 and PtRu215, respectively.

Fig. 4.18 shows the effect of hydrogen dilution with nitrogen. The behavior was standard and corresponded to the other samples. However, the whole measeurement was affected by sample degradation which was much faster than for Pt103 and Pt113. The power dropped to less than 30 % of its initial value in ten hours and it did not restore, not even after cyclic voltammetry. Same behavior was observed for PtRu123.

5. Discussion

5.1 General comparison of the samples

The performance of all samples under normal conditions, i.e. pure hydrogen without any impurities, is summarized in Tab. 5.1. Three samples - Reference, Pt105, PtRu115 - showed maximum power around 4 W, see Fig. 5.1. In the case of Pt105, this value was reached after cyclic voltammetry and in the case of PtRu115 almost five days after break-in. The possitive effect of cyclic voltammetry and following enhancement could be easily explained by electrochemical cleaning of the catalyst and an increase of the electrochemically active surface area. On the other hand, the behavior of PtRu115 is difficult to understand and a more detailed chemical analysis would be required to find an explanation.

the fifth column in the Tab. 5.1 represents voltage at which maximum power occured. It is affected especially by reaction rate and inner resistance of the cell. An optimal value for applications is around 500 mV. The data show an interesting phenomenon: all samples with a 0.3 cathode reached maximum power at higher voltage than the equivalent samples with a 0.5 cathode.

Statistical error linked with actual state of the system in the time of measurements and its instability represents the dominant part of the uncertainty of values given in Tab. 5.1. Systematical error of load is, in comparison with statistical error, negligible. Given the observed stability and behavior of the samples, the uncertainty could be estimated to 100 mW. However, due to the very long times needed for each series of measurements, each of the samples was measured only once. Thus a repetition of these experiments is required to fully prove all observations.

The catalyst had a square shape with a side of 2.1 cm. Power density was calculated by dividing maximum power by 4.41 cm^2. Values around 900 mW/cm^2 are comparable with or slightly less than those obtained in a previous work carried out at our departement [48, 47] and a commercially acceptable standard which is around 1 W/cm^2.

Nowadays, specific power, i.e. power per amount of platinum, is not a crucial

Sample	Pt:Ru	Cath.	MP[mW]	U[mV]	PD[mW/cm^2]	SP[mW/mg]
Reference	-	0.5	3965	550	899	1124
Pt103	-	0.3	2295	621	520	1577
Pt105	-	0.5	2442	479	554	1045
			3867	527	877	1654
PtRu113	1:1	0.3	2040	621	463	1402
PtRu115	1:1	0.5	2644	474	600	1131
			4072	493	923	1742
PtRu123	1:2	0.3	1265	502	287	869
PtRu125	1:2	0.5	2127	451	482	910
PtRu215	2:1	0.5	2866	578	650	1226

Table 5.1: Summary of the performance of all samples under normal conditions. The type of cathode - 0.3 mgPt/cm^2 and 0.5 mgPt/cm^2 is in the third column, the other abbreviations stand for: MP - maximum power, PD - power density, SP - specific power per miligram of platinum

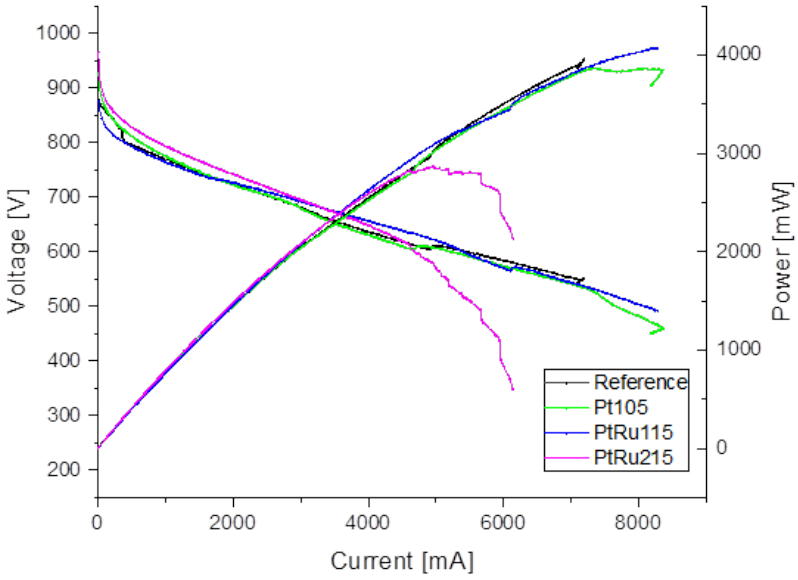

Figure 5.1: IV curves of Reference, Pt105, PtRu115 and PtRu215

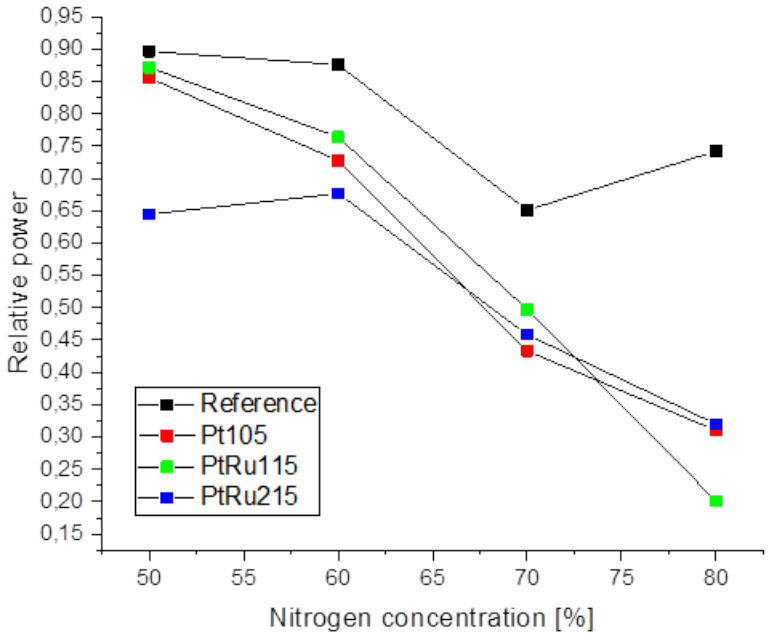

Figure 5.2: Hydrogen dilution with nitrogen - comparison of samples

parameter, and the stability and CO tolerance is much more relevant. However, it could be a good secondary criterium for the evaluation of the catalyst quality. Specific power of our samples was up to 50 % higher than the one of the reference. However, this value is strongly affected by "high" platinum loading of the cathode. If only anode loading was considered, specific power of our samples would be five to ten times higher than that of the reference.

5.2 Effect of nitrogen

All samples except the reference showed the same behavior during hydrogen dilution or more specifically during a replacement of a part of hydrogen with nitrogen. A comparison of the four best samples is given in Fig. 5.2. A decrease in power with increasing nitrogen concentration is mostly linear. However, there is no simple physical argument for this type of behavior. Diffusion and reaction kinetics are definitely affected by hydrogen concentration, but to find the real dependence, which might be more complicated, further detailed analysis (e.g. impedance spectroscopy to determine coeficients of reaction kinetics) is in place.

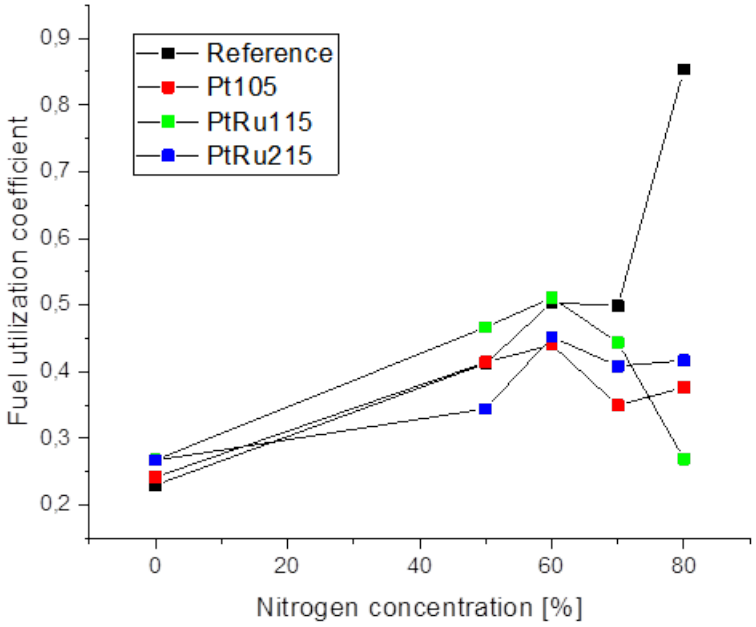

Figure 5.3: Fuel utilization coefficient for nitrogen concentrations from 50 % to 80 %

The power decrease in the case of reference could be also linear, but with a smaller slope.

The power drop is most probably caused by lack of hydrogen. Theoretically according to Eq. (2.6), 16 sccm of hydrogen corresponding to the presence of 80 % of nitrogen should be sufficient for current above 2 A. However, in this calculation, we assume that all injected hydrogen contributes to the current. The real values of fuel utilization coefficient are shown in Fig. 5.3. With 80 sccm of pure hydrogen, the most limiting factor is the reaction rate. There is an excess of fuel and the reaction is able to consume only a small part of it, which results in μ coefficient between $0.2 - 0.3$. Fuel utilization coefficient is slowly growing with hydrogen dilution up to $0.4 - 0.5$ at 60 % of nitrogen and then it starts to decrease. This is not the case of reference, which at 80 % of nitrogen reached fuel utilization of 0.9. Potential explanation is related to diffusion of hydrogen. At high nitorgen concentrations, hydrogen is too diluted that most of it does not reach the platinum site and it is carried away from the cell by nitrogen flow instead. The reference, on the other hand, contains ten times more platinum and

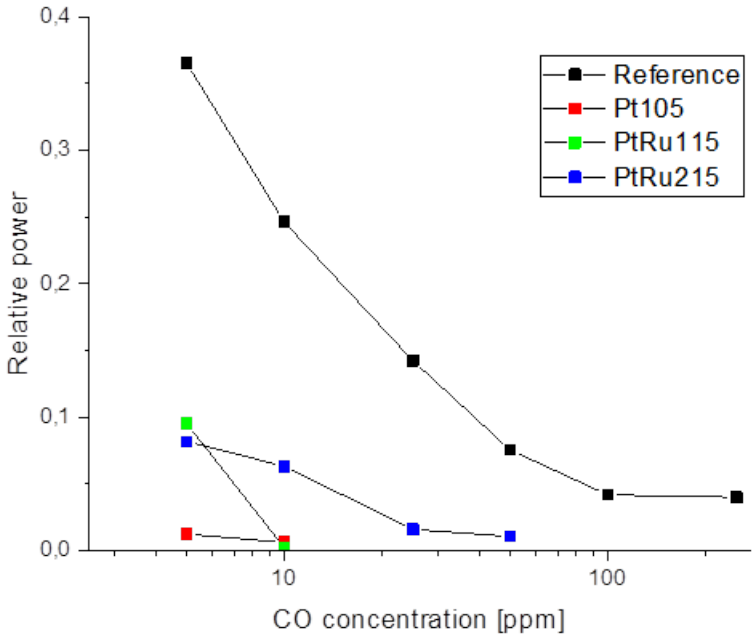

Figure 5.4: Effect of exposure to different CO concentration

its structure is different. While our catalysts are sputtered directly on membrane, the commercial one is made of powder and placed on a microporous layer and thus hydrogen can more easily access the active sites.

Effect of changes of hydrogen partial pressure with the addition of nitrogen to constant hydrogen flow was not observed, even though Eq. (2.10) says that a reversible potential between electrodes should decrease with it. However, the decrease should be in the order of a few percent, which is under our resolution limit due to the instabilities and oscillations caused by water management.

5.3 CO poisoning

It was proved that even small amount of CO present in the fuel has a dramatic effect on the fuel cell performance. Fig. 5.4 shows the relative power of the individual samples during exposure to different CO concentrations. Clearly, the CO tolerance of our low platinum loading catalysts is significantly worse than of the commercial one with high platinum loading. Of all sputtered layers, the best result was obtained for PtRu215. PtRu115 was also promising, however, it never

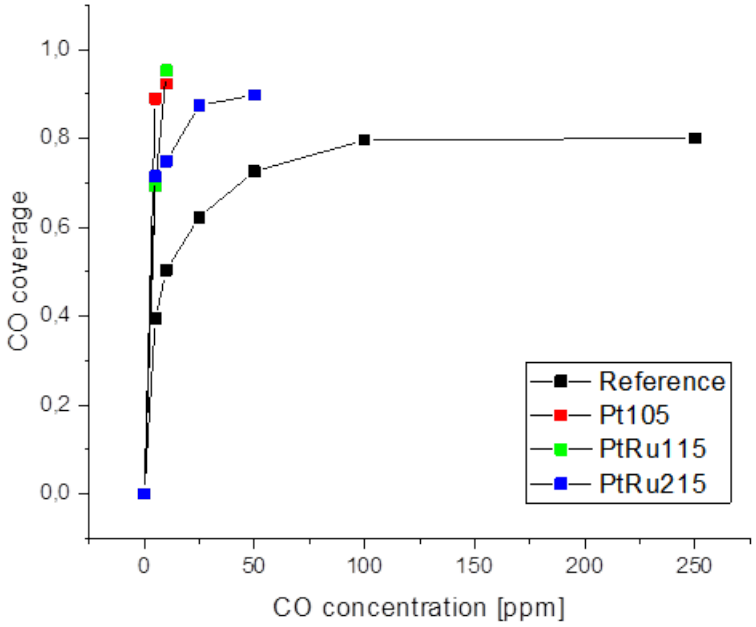

Figure 5.5: Dependence of CO coverage on concentration

reached the initial values of power during recovery cycles.

The main difference between the samples with different PtRu ratio was CO tolerance and also the time and efficiency of the recovery. Pure platinum samples were extremely sensitive to even the smallest tested CO concentration, their recovery took a long time, and cyclic voltammetry had to be used to fully restore initial power and stability. On the other, an excess of ruthenium is counterproductive. Both PtRu123 and PtRu125 exhibited weak stability, low performance and short lifetime. The ideal ratio lays under 50% of ruthenium which is in agreement with previous studies e.g. [44].

CO coverage was calculated using Eq. (2.15) and its dependance on CO concentration is plotted in Fig. 5.5. The curves for the reference and sample PtRu215 follow the Langmuir isotherm equation:

$$\theta = A \cdot \frac{kp}{1 + kp}, \tag{5.1}$$

where A and k stands for coefficient and p is the partial pressure of CO, which, in our case, corresponds to CO concentration. This shows that the power drop is caused by the creation of a monolayer of CO adsorbed on platinum sites.

5.4 Combined effect of nitrogen and CO

A simultaneous decrease in hydrogen and CO partial pressure showed two different types of behavior. The first one was observed with the reference (Fig. 4.4) and sample PtRu115 (Fig. 4.14) and the power remained constant or slighly increased. On the other hand, Pt105 (Fig. 4.9) showed a strong dependance on any change in the fuel composition. This sample appeared to have the worst CO tolerance and thus its sensitivy to impurities could be expected. However, it does not explain the almost negligible reaction of the two other samples.

The second experiment with nitrogen and CO partly fulfilled our expectations. The power decreased but more that it was expected, especially for the reference (Fig. 4.5) and sample Pt105 (Fig. 4.10). This has been already observed and modeled with the conclusion that the effect of nitrogen and CO "magnify" each other resulting in higher power drop [49].

Another possible explanation of both experiments with simoultaneous exposure to CO and nitrogen is based on the hypothesis that the ratio of hydrogen and CO plays a more important role than the CO partial pressure. According to the observed behavior of sample Pt105, see Fig. 4.9, the hypothesis might be valid only for CO concentration lower than poisoning threshold. On the other hand, for concetrations above poisoning threshold, CO partial pressure dominates. However, this hypothesis is based on only three measurements and further study with different samples and CO concentrations is required to understand this phenomenon and thus it remains an open question. Except for one model study [49] and a few experimental studies [49, 50] no paper dealing with this topic have been published.

6. Conclusion

The aim of this thesis was to study the effect of the presence of CO and nitrogen in the fuel on the performance of PEMFC. For these purposes, an extention of testing station for two-step mixing of gases was successfully constructed and tested. The reference sample with commercial electrodes, and a set of samples with two types of commercial cathodes and a home-made anode deposited by magnetron sputtering on etched membrane with different platinum-ruthenium ratio were studied.

The commercial cathode with platinum loading of 0.3 $\mathrm{mgPt/cm^2}$ showed lower power and stability than the 0.5 $\mathrm{mgPt/cm^2}$ cathode. Furthermore, it had a short lifetime and approximately after one week it started to degrade.

Nitrogen showed to be innert and it has no effect except for the dilution of hydrogen. During this experiment, fuel utilization was studied. Fuel utilization coefficient probably depends on the reaction rate and also on the structure and diffusive properties of the anode.

Addition of a small amount of CO to the hydrogen results in a significant decrease of power. CO concentration as low as 5 ppm caused a power drop higher than 50 % for all samples including the commercial reference, and for some samples even more than 90 %. It was shown that low platinum content catalysts has a higher sensitivity to any impurities in the fuel and lower CO tolerance.

Different platinum ruthenium ratio was tested to enhance the CO tolerance. An excess of ruthenium (PtRu ratio 1:2) was counterproductive and lead to low power, instability and short lifetime of the samples. The best results was reached with PtRu ratio 2:1. The power densities with this ratio were lower than for the reference, but the CO tolerance was the best of all sputtered samples; however, not better than commercial anode. This is supposed to be due to a much higher platinum loading (0.3 $\mathrm{mgPt/cm^2}$) in comparison with our sputtered samples. Commercially recognized, or at least the most available, 1:1 PtRu ratio showed the best power, but slightly worse CO tolerance and problems with restoring initial value of power after CO exposure.

A combined effect of nitrogen and CO was also studied. The results of simul-

taneous decrease of CO and hydrogen partial pressure suggests that the ratio of CO and hydrogen is more a crucial parameter for CO concentration bellow the poisoning threshold; for higher concentrations CO partial pressure is dominating. Experiments with constant CO partial pressure and various CO-hydrogen ratio were in agreement with this hypothesis. The negative effects of nitrogen and CO presence in the fuel enhanced one another, which has been already described, although not fully explained in the literature. However, only three samples were measured and the results were not completely conclusive, thus more detailed analysis is required.

Bibliography

[1] da Silva Veras T, Simonato Mozer T, da Costa Rubim Messeder dos Santos D, and da Silva César A. Hydrogen: Trends, production and characterization of the main process worldwide. *International Journal of Hydrogen Energy*, 42(4):2018–2033, jan 2017.

[2] Baschuk JJ and Li X. Carbon monoxide poisoning of proton exchange membrane fuel cells. *International Journal of Energy Research*, 25(8):695–713, 2001.

[3] Yuan X-Z and Wang H. *PEM Fuel Cell Electrocatalysts and Catalyst Layers - Fundamentals and Applications*, chapter 1. PEM Fuel Cell Fundamentals, pages 1–88. Springer, 2008.

[4] Appleby AP. From sir william grove to today: Fuel cells and the future. *Journal of Power Sources*, 29:3–11, 1990.

[5] Grimwood JM; Hacker CB and Vorzimmer PJ. *Project Gemini - Technology and Operations*. Scientific and Information Division, Office of Technology Utilization, National Aeronautics and Space Administration, 1969.

[6] Fitzgerald J and O'Brien N. Fuel cells: A better energy source for earth and space. online, November 2005. https : //www.nasa.gov/centers/glenn/technology/fuel_cells.html.

[7] Resnick PR. A short history of nafion. *Actualite Chimique*, pages 144–147, 2006.

[8] Ballard milestones. online. http://www.ballard.com/about-ballard/our-history.

[9] National Institute of Standards and Technology. Water. online. https://webbook.nist.gov/cgi/cbook.cgi?ID=C7732185&Units=SI&Mask=2#Thermo-Condensed.

[10] Nguyen TV and White RE. A water and heat management model for proton-exchange-membrane fuel cells. *Journal of The Electrochemical Society*, 140(8):2178, 1993.

[11] Fuller TF and Newman J. Water and thermal management in solid-polymer-electrolyte fuel cells. *Journal of The Electrochemical Society*, 140(5):1218, 1993.

[12] Pasaogullari U and Wang C-Y. Two-phase transport and the role of micro-porous layer in polymer electrolyte fuel cells. *Electrochimica Acta*, 49(25):4359–4369, oct 2004.

[13] Liu X, Peng F, Lou G, and Wen Z. Liquid water transport characteristics of porous diffusion media in polymer electrolyte membrane fuel cells: A review. *Journal of Power Sources*, 299:85–96, dec 2015.

[14] Pilatowsky I, Romero RJ, Isaza CA, Gamboa SA, Sebastian PJ, and Rivera W. *Cogeneration Fuel Cell - Sorption Air Conditioning Systems*, chapter 2 - Termodynamics of Fuel Cells. Springer, 2011.

[15] Colak OU and Acar A. Modeling of hydro-thermo-mechanical behavior of nafion NRE212 for polymer electrolyte membrane fuel cells using the finite viscoplasticity theory based on overstress for polymers (FVBOP). *Mechanics of Time-Dependent Materials*, 17(3):331–347, sep 2012.

[16] Open chemistry database - nafion. online. cited 15.02.2019. *https* : *//pubchem.ncbi.nlm.nih.gov/compound/*61889*#section* = *Top*.

[17] Mauritz KA and Moore RB. State of understanding of nafion. *Chemical Reviews*, 104(10):4535–4586, oct 2004.

[18] Hsu WY and Gierke TD. Ion transport and clustering in nafion perfluorinated membranes. *Journal of Membrane Science*, 13(3):307–326, feb 1983.

[19] Heinzel A and Barragán VM. A review of the state-of-the-art of the methanol crossover in direct methanol fuel cells. *Journal of Power Sources*, 84(1):70–74, nov 1999.

[20] Inaba M, Kinumoto T, Kiriake M, Umebayashi R, Tasaka A, and Ogumi Z. Gas crossover and membrane degradation in polymer electrolyte fuel cells. *Electrochimica Acta*, 51(26):5746–5753, aug 2006.

[21] Weber AZ. Gas-Crossover and Membrane-Pinhole Effects in Polymer-Electrolyte Fuel Cells. *Journal of The Electrochemical Society*, 155(6):B521, 2008.

[22] Zhang H, Li J, Tang H, Lin Y, and Pan M. Hydrogen crossover through perfluorosulfonic acid membranes with variable side chains and its influence in fuel cell lifetime. *International Journal of Hydrogen Energy*, 39(28):15989–15995, sep 2014.

[23] Durst J, Simon C, Hasché F, and Gasteiger HA. Hydrogen oxidation and evolution reaction kinetics on carbon supported pt, ir, rh, and pd electrocatalysts in acidic media. *Journal of The Electrochemical Society*, 162(1):F190–F203, dec 2014.

[24] Kumar A and Reddy RG. Effect of channel dimensions and shape in the flow-field distributor on the performance of polymer electrolyte membrane fuel cells. *Journal of Power Sources*, 113(1):11–18, jan 2003.

[25] Dicks AL. The role of carbon in fuel cells. *Journal of Power Sources*, 156(2):128–141, jun 2006.

[26] Wang H, Sweikart MA, and Turner JA. Stainless steel as bipolar plate material for polymer electrolyte membrane fuel cells. *Journal of Power Sources*, 115(2):243–251, apr 2003.

[27] Mehta V and Cooper JS. Review and analysis of PEM fuel cell design and manufacturing. *Journal of Power Sources*, 114(1):32–53, feb 2003.

[28] Ramousse J, Didierjean S, Lottin O, and Maillet D. Estimation of the effective thermal conductivity of carbon felts used as PEMFC gas diffusion layers. *International Journal of Thermal Sciences*, 47(1):1–6, jan 2008.

[29] He G, Yamazaki Y, and Abudula A. A three-dimensional analysis of the effect of anisotropic gas diffusion layer(GDL) thermal conductivity on the

heat transfer and two-phase behavior in a proton exchange membrane fuel cell(PEMFC). *Journal of Power Sources*, 195(6):1551–1560, mar 2010.

[30] Falcão DS, Oliveira VB, Rangel CM, Pinho C, and Pinto AMFR. Water transport through a PEM fuel cell: A one-dimensional model with heat transfer effects. *Chemical Engineering Science*, 64(9):2216–2225, may 2009.

[31] Zhang FY, Yang XG, and Wang CY. Liquid water removal from a polymer electrolyte fuel cell. *Journal of The Electrochemical Society*, 153(2):A225, 2006.

[32] Platinum based electrodes. onlilne. https://www.fuelcellstore.com/fuel-cell-components/gas-diffusion-electrode/platinum-electrodes. cited 2019/03/13.

[33] Wang B. Recent development of non-platinum catalysts for oxygen reduction reaction. *Journal of Power Sources*, 152:1–15, dec 2005.

[34] Dhar HP. Performance study of a fuel cell pt-on-c anode in presence of CO and CO[sub 2], and calculation of adsorption parameters for CO poisoning. *Journal of The Electrochemical Society*, 133(8):1574, 1986.

[35] Solla-Gullón J, Vidal-Iglesias FJ, Herrero E, Feliu JM, and Aldaz A. CO monolayer oxidation on semi-spherical and preferentially oriented (100) and (111) platinum nanoparticles. *Electrochemistry Communications*, 8(1):189–194, jan 2006.

[36] de Becdelièvre AM, de Becdelièvre J, and Clavilier J. Electrochemical oxidation of adsorbed carbon monoxide on platinum spherical single crystals. *Journal of Electroanalytical Chemistry and Interfacial Electrochemistry*, 294(1-2):97–110, nov 1990.

[37] Oetjen HF. Performance data of a proton exchange membrane fuel cell using h2/co as fuel gas. *Journal of The Electrochemical Society*, 143(12):3838, 1996.

[38] Cheng X, Shi Z, Glass N, Zhang L, Zhang J, Song D, Liu Z-S, Wang H, and Shen J. A review of PEM hydrogen fuel cell contamination: Impacts, mechanisms, and mitigation. *Journal of Power Sources*, 165(2):739–756, mar 2007.

[39] Singh M, Moore J, and Shadis W. Hydrogen Demand, Production, and Cost by Region to 2050. online, August 2005. http://www.osti.gov/bridge.

[40] Ewan B and Allen R. A figure of merit assessment of the routes to hydrogen. *International Journal of Hydrogen Energy*, 30(8):809–819, jul 2005.

[41] Li Q, He R, Jensen JO, and Bjerrum NJ. Approaches and recent development of polymer electrolyte membranes for fuel cells operating above 100°C. *Chemistry of Materials*, 15(26):4896–4915, dec 2003.

[42] Gottesfeld S and Pafford J. A new approach to the problem of carbon monoxide poisoning in fuel cells operating at low temperatures. *Journal of The Electrochemical Society*, 135(10):2651, 1988.

[43] Bernardi DM and Verbrugge MW. A mathematical model of the solid-polymer-electrolyte fuel cell. *Journal of The Electrochemical Society*, 139(9):2477, 1992.

[44] Ianniello R, Schmidt VM, Stimming U, Stumper J, and Wallau A. CO adsorption and oxidation on pt and ptru alloys: dependence on substrate composition. *Electrochimica Acta*, 39(11-12):1863–1869, aug 1994.

[45] Wee JH and Lee KY. Overview of the development of CO-tolerant anode electrocatalysts for proton-exchange membrane fuel cells. *Journal of Power Sources*, 157(1):128–135, jun 2006.

[46] Magnetron sputtering. online. https://physics.mff.cuni.cz/kfpp/povrchy/method/ms.

[47] Fiala R. *Investigation of new catalysts for polymer membrane fuel cells.* PhD thesis, Department of Surface and Plasma Science, Charles University, Prague, 2017.

[48] Ostroverkh A, Dubau M, Johánek V, Václavů M, Šmíd B, Veltruská K, Ostroverkh Y, Fiala R, and Matolín V. Efficient Pt-C MEA for PEMFC with Low Platinum Content Prepared by Magnetron Sputtering. *Fuel Cells*, 18(1):51–56, feb 2018.

[49] Wang W, Wang W, and Chen S. The effects of hydrogen dilution, carbon monoxide poisoning for a pt–ru anode in a proton exchange membrane fuel cell. *International Journal of Hydrogen Energy*, 41(45):20680–20692, dec 2016.

[50] Chen C-Y, Lai W-H, Yan W-M, Chen C-C, and Hsu S-W. Effects of nitrogen and carbon monoxide concentrations on performance of proton exchange membrane fuel cells with pt–ru anodic catalyst. *Journal of Power Sources*, 243:138–146, dec 2013.

List of Figures

List of Tables